

DIS on a Large Nucleus in AdS/CFT

Javier L. Albacete, Yuri V. Kovchegov, Anastasios Taliotis

Department of Physics, The Ohio State University, Columbus, OH 43210, USA

E-mail addresses: albacete@mps.ohio-state.edu, yuri@mps.ohio-state.edu,
taliotis.1@osu.edu

ABSTRACT: We calculate the total cross section for deep inelastic scattering (DIS) on a nucleus at high energy for a strongly coupled $\mathcal{N} = 4$ super Yang-Mills theory using AdS/CFT correspondence. In analogy to the small coupling case we argue that at high energy the total DIS cross section is related to the expectation value of the Wilson loop formed by the quark–antiquark dipole. We model the nucleus by a metric of a shock wave in AdS₅. We then calculate the expectation value of the Wilson loop by finding the extrema of the Nambu-Goto action for an open string attached to the quark and antiquark lines of the loop in the background of an AdS₅ shock wave. We find three extrema of the Nambu-Goto action: the string coordinates at the extrema are complex-valued and are given by three different branches of the solution of a cubic equation. The physically meaningful solutions for the total DIS cross section are given either by the only branch with a purely imaginary string coordinate in the bulk or by a superposition of the two other branches. For both solutions we obtain the forward scattering amplitude N for the quark dipole–nucleus scattering. We study the onset of unitarity with increasing center-of-mass energy and transverse size of the dipole: we observe that for both solutions the saturation scale, while energy-dependent at lower energies, at very high energy becomes independent of energy/Bjorken- x . The saturation scale depends very strongly on the atomic number of the nucleus as $Q_s \sim A^{1/3}$.

KEYWORDS: AdS/CFT correspondence, Deep Inelastic Scattering, Saturation.

Contents

1. Introduction	1
2. Setting up the Problem	4
3. Static Solution	10
4. Evaluating the S-matrix	15
4.1 General Evaluation	15
4.2 Single Branch	19
4.3 Superposition of Two Branches	23
5. Conclusions	27
A. Monotonicity of $N(r, s)$ as a function of r	29

1. Introduction

Over the past years there has been some significant progress made in our understanding of deep inelastic scattering (DIS) at high energy/small Bjorken- x in the framework of the Color Glass Condensate (CGC) [1, 2, 3, 4, 5, 6, 7, 8, 9, 10, 11, 12, 13, 14, 15, 16, 17, 18, 19, 20, 21, 22, 23, 24]. It was shown that at moderately small x_{Bj} the total DIS cross section is well-described in the quasi-classical (Glauber–Mueller (GM)/McLerran–Venugopalan (MV)) [25, 3, 4, 5] approximation including all multiple rescatterings each taken at the lowest (two-gluon) order. At smaller x_{Bj} the energy-dependence of the cross section comes in through the non-linear small- x_{Bj} Balitsky–Kovchegov (BK) [19, 20, 21, 17, 18] and Jalilian-Marian–Iancu–McLerran–Weigert–Leonidov–Kovner (JIMWLK) [9, 10, 11, 12, 13, 14, 15, 16] quantum evolution equations. The BK and JIMWLK evolution equations unitarize the linear Balitsky–Fadin–Kuraev–Lipatov (BFKL) [26, 27] evolution equation at high energies in the large- N_c limit (BK) and beyond (JIMWLK).

The main principle of the CGC approach is the existence of a momentum scale Q_s , called the saturation scale, which regulates the infrared divergences in the total DIS cross section and in other relevant observables for high energy collisions (for a review see [22, 23, 24]). The saturation scale grows as a power of the center-of-mass energy of the collision (a power of Bjorken x) as follows from BK and JIMWLK equations, and as a power of the atomic number A for DIS on the nucleus, as can

be seen in the quasi-classical GM and MV approaches. More specifically, for small- x_{Bj} evolution at the leading logarithmic ($\alpha_s \ln 1/x_{Bj}$) approximation (LLA) at fixed coupling $Q_s^2 \sim (1/x_{Bj})^\delta \alpha_s A^{1/3}$, where α_s is the strong coupling constant and $\delta \approx 4.8$ [28, 29]. Thus at high energies and/or for large nuclei the saturation scale can be large, much larger than Λ_{QCD} , cutting off the non-perturbative infrared (IR) effects. This justifies the perturbative approach and makes CGC physics perturbative.

While the picture described above is theoretically robust and self-consistent, the physics of CGC has not yet reached the level of precision required to make unambiguous phenomenological predictions. The fixed coupling LLA approaches, while giving interesting qualitative predictions confirmed by HERA and RHIC data [30, 31, 32, 33, 34, 35, 36], require many additional assumptions to describe the data quantitatively. At the same time it is known that NLO corrections to the BFKL kernel (and therefore to BK and JIMWLK kernels as well) are large [37, 38, 39]. They come in with a sign opposite to that of the LLA kernel, leading to cross sections decreasing with energy and other undesirable consequences [40, 41]. It is believed that resummation of all higher order corrections should remedy this problem. This idea is supported by the success of resummation of collinear singularities in the all-order BFKL kernel performed in [42]. Recent calculation of the running coupling corrections to the BFKL, BK and JIMWLK [43, 44, 45, 46] and the resulting successful phenomenology both for DIS and for heavy ion collisions at RHIC [36, 47] also support the possibility that resummation of all higher order corrections to BK and JIMWLK evolution equations would improve the agreement with the data and resolve theoretical problems posed by NLO BFKL calculation.

While it is not clear at all how to resum higher order corrections to the BK and JIMWLK kernels to all orders in QCD, one turns for guidance to other QCD-like theories, such as $\mathcal{N} = 4$ super Yang–Mills (SYM), where one can perform calculations in the non-perturbative limit of large 't Hooft coupling due to the Anti-de Sitter space/conformal field theory (AdS/CFT) correspondence [48, 49, 50, 51]. The original work in this direction was performed by Janik and Peschanski [52] (see also [53, 54, 55, 56]), who showed that at large 't Hooft coupling the scattering cross section mediated by a single pomeron exchange, corresponding to a single graviton exchange in the bulk of AdS_5 , grows as the first power of energy, $\sigma_{\text{tot}} \sim s$. Comparing this result to the LLA BFKL prediction at small coupling of $\sigma_{\text{tot}} \sim s^{\frac{4\alpha_s N_c}{\pi} \ln 2}$ [26, 27], which is the same for both QCD and $\mathcal{N} = 4$ SYM being entirely due to gluon dynamics, one concludes that the power of energy changes from 0 to 1 as 't Hooft coupling $\lambda = 4\pi \alpha_s N_c$ goes from being small to being large. The result of [52] was further expanded in [57]. It also agrees with the extrapolation of the results of weak coupling resummations [58]. The conclusion one may draw from these results is that the cross sections should grow fastest with energy when the coupling is large. However, as in QCD the coupling is large at low momentum transfer Q^2 , one would conclude that the cross section should grow steeper with s as Q^2 gets lower. Such conclusion would completely contradict the existing DIS and proton-proton collisions phenomenology [59], which shows that the exact opposite is true: the growth of cross sections with energy slows down with decreasing Q^2 .

We believe the resolution of this puzzle may lie in the physics of parton saturation/CGC. As one goes towards lower Q^2 , single-pomeron exchange approximation becomes invalid, and one has to resum multiple pomeron exchanges. These exchanges unitarize the total cross section, significantly reducing its growth with energy [24]. Hence to make the strongly-coupled dynamics consistent with phenomenology, saturation/CGC effects need to be included in the picture as well. The first steps in this direction were performed in [60, 61], where the authors studied DIS on a static $\mathcal{N} = 4$ SYM at strong coupling by calculating a correlator of two R -currents. Here we will present a different approach to DIS in AdS. We will argue below that the total DIS cross section at high energy can be related to an expectation value of the Wilson loop formed by the propagators of a quark and an anti-quark arising in the splitting of the incoming virtual photon. The expectation value of a Wilson loop can be found at strong coupling using the methods outlined in [62] (see also [63, 64, 65]). We will model the nucleus by a shock wave metric in AdS_5 . The expectation value of the Wilson loop in the shock wave background is related to value of the Nambu-Goto action at the extremal string world-sheet [62] for an open string connecting the quark and the anti-quark lines. We therefore extremize the open string action. Our calculation is similar to those performed in [66, 67, 68, 69, 70, 71, 72, 73, 74, 75]. We obtain the expectation value of the Wilson loop, which is easily related to the forward scattering amplitude $N(\mathbf{r}, Y)$ of a $q\bar{q}$ dipole of transverse size \mathbf{r} on the nuclear target with the total rapidity interval of $Y \sim \ln s \sim \ln 1/x_{Bj}$. The obtained $N(\mathbf{r}, Y)$ is unitary and exhibits saturation transition when the dipole transverse size becomes sufficiently large. We extract the saturation scale from the obtained expression and notice that at very high scattering energy s , corresponding to large Y or small Bjorken- x , the saturation scale becomes independent of energy, contrary to the perturbative behavior outlined above.

The paper is structured as follows. In Sect. 2 we discuss the relation of the total DIS cross section to the expectation value of a Wilson loop. We set up the problem in AdS_5 space and introduce the shock wave metric. We look for the extrema of the open string connecting the quark and the anti-quark in the shock wave background in Sect. 3. We argue in Sect. 3 that for broad enough shock waves the Nambu-Goto action is dominated by static string configurations. Such approximation is justified for scattering on nuclei with sufficiently large atomic number A . We solve the static equations of motion for the open string and find that there are three possible complex-valued solutions for string coordinates extremizing Nambu-Goto action in the presence of the shock wave. Similar results are usually obtained in the quasi-classical approximation in quantum mechanics (see Ch. 131 in [76]). In the context of AdS/CFT similar properties have been found in [77].

We study the forward scattering amplitudes $N(\mathbf{r}, Y)$ (or, equivalently, the S -matrices $S(\mathbf{r}, Y)$), resulting from these solutions in Sect. 4. We notice that only one branch of the solution gives a physically meaningful unitary non-negative $N(\mathbf{r}, Y)$ for all \mathbf{r} and Y . The branch has purely imaginary string coordinates in the bulk. The corresponding $N(\mathbf{r}, Y)$ is given by Eq. (4.14) and is plotted in Fig. 7. We notice that a slight modification of Maldacena's prescription for the calculation

of Wilson loops shown in Eq. (4.29) allows for a combination of two other branches to also give a meaningful and physical amplitude $N(\mathbf{r}, Y)$. The resulting amplitude is shown in Eq. (4.30) and is plotted in Fig. 9.

The saturation scale Q_s as a function of center-of-mass energy s is found in Sect. 4 as well and is shown in Figs. 8 and 10 for both solutions. For both solutions it appears that at intermediate energies the saturation scale grows with s . However the growth of Q_s with s stops at very high energies, reminiscent of “saturation of saturation” conjectured in [78]. We try to interpret this result in Sect. 5, where we also plot the resulting behavior of the saturation scale in the strong coupling sector of QCD in Fig. 11.

2. Setting up the Problem

In DIS at high energies, when viewed in the target rest frame, the incoming virtual photon splits into a quark-antiquark pair, which then scatters on the proton or nuclear target [79, 25, 80]. The process is depicted in Fig. 1. The scattering of a $q\bar{q}$ pair on the target is eikonal at high energies [79, 25, 80, 17]. The light-cone lifetime of the $q\bar{q}$ pair is much longer than the nuclear radius. Using light-cone perturbation theory [81, 82] one can therefore decompose the total scattering cross section of DIS into a convolution of a light-cone wave function squared (Φ) for a virtual photon to decay into a $q\bar{q}$ pair and the imaginary part of the forward scattering amplitude for the $q\bar{q}$ pair–target interaction (N) [79, 25, 17]:

$$\sigma_{tot}^{\gamma^*A}(Q^2, x_{Bj}) = \int \frac{d^2r d\alpha}{2\pi} \Phi(\mathbf{r}, \alpha, Q^2) d^2b N(\mathbf{r}, \mathbf{b}, Y). \quad (2.1)$$

Here $N(\mathbf{r}, \mathbf{b}, Y)$ is the imaginary part of the forward scattering amplitude for the scattering of a quark-antiquark dipole of transverse size \mathbf{r} at center-of-mass impact parameter \mathbf{b} on a target, where the total rapidity of the scattering process is $Y = \ln 1/x_{Bj}$ with x_{Bj} the Bjorken x variable. $\Phi(\mathbf{r}, \alpha)$ is the light-cone wave function squared of the virtual photon with virtuality Q^2 splitting into a $q\bar{q}$ pair of transverse size \mathbf{r} with the quark carrying a fraction α of the virtual photon’s longitudinal (plus) momentum. (Boldface notation denotes two-dimensional vectors in the transverse plane.)

It is important to stress that the factorization of Eq. (2.1) is independent of the strong interaction dynamics. The wave function squared $\Phi(\mathbf{r}, \alpha, Q^2)$ is purely due to electromagnetic interactions, and is very well known [79, 83, 24]. All the strong interaction dynamics is contained in $N(\mathbf{r}, \mathbf{b}, Y)$.

In perturbation theory, at the leading logarithmic level in $\alpha_s \ln 1/x_{Bj}$, the scattering between the $q\bar{q}$ pair and the target is eikonal. One can therefore relate $N(\mathbf{r}, \mathbf{b}, Y)$ to the expectation value of a fundamental Wilson loop [19, 21, 17, 18, 14]

$$N(\mathbf{r}, \mathbf{b}, Y) = 1 - S(\mathbf{r}, \mathbf{b}, Y) \quad (2.2)$$

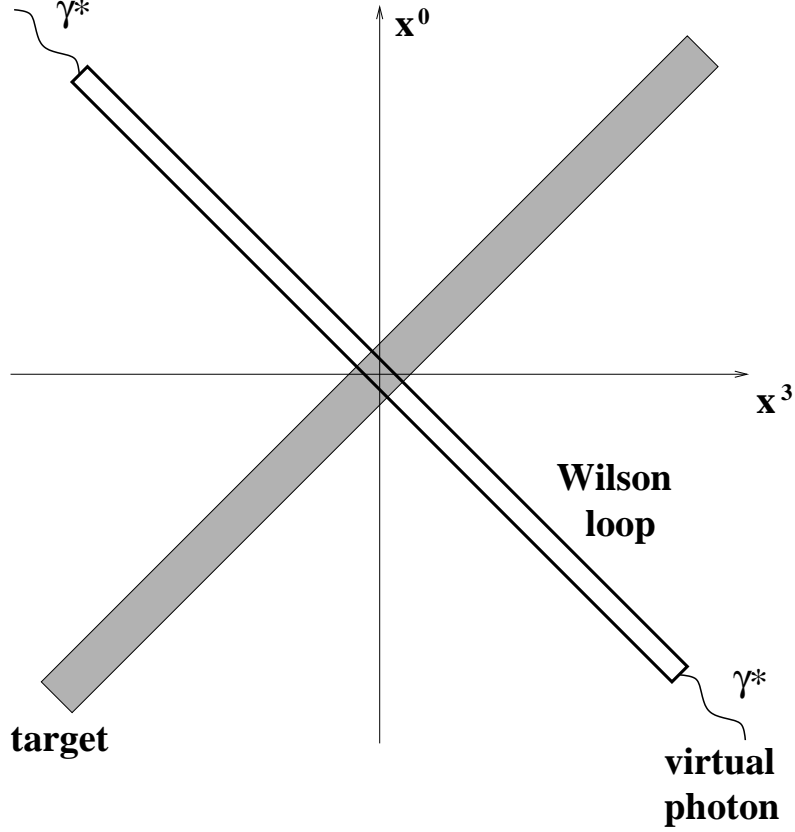


Figure 1: The space-time picture of the forward amplitude for the deep inelastic scattering (DIS) at high energy. The collision axis is labeled x^3 , the time is x^0 . The virtual photon (γ^*) travels along one light cone and splits into a Wilson loop. The $q\bar{q}$ pair in the loop is separated only in the transverse plane: the separation shown along the x^3 -direction is for illustration purposes only. The Wilson loop then scatters on the target, traveling along the other light cone. As it is a forward amplitude, $q\bar{q}$ pair recombines back into γ^* after the scattering.

with the (real part of the) S -matrix

$$S(\mathbf{r}, \mathbf{b}, Y) = \frac{1}{N_c} \text{Re} \left\langle W \left(\mathbf{b} + \frac{1}{2}\mathbf{r}, \mathbf{b} - \frac{1}{2}\mathbf{r}, Y \right) \right\rangle. \quad (2.3)$$

$W(\mathbf{b} + \frac{1}{2}\mathbf{r}, \mathbf{b} - \frac{1}{2}\mathbf{r}, Y)$ denotes a Wilson loop formed out of a quark line at $\mathbf{b} + \frac{1}{2}\mathbf{r}$ and an antiquark line at $\mathbf{b} - \frac{1}{2}\mathbf{r}$ with the links connecting the two lines at plus and minus infinities on the light cone. In the frame where the target is at rest, the Wilson loop is oriented close to the light cone, with rapidity Y reflecting the “angle” with respect to the light cone [19, 21]. The averaging in Eq. (2.3), denoted by $\langle \dots \rangle$, is performed over all possible wave functions of the target.

Neglecting the gauge links at the light-cone infinities by choosing an appropriate gauge, in QCD perturbation theory the Wilson loop can be rewritten in terms of Wilson lines [9, 10, 11, 12, 13, 14,

15, 16, 19, 21]

$$W(\mathbf{x}, \mathbf{y}, Y) = \text{tr}[U(\mathbf{x}, Y) U^\dagger(\mathbf{y}, Y)] \quad (2.4)$$

where the Wilson line is

$$U(\mathbf{x}, Y) = \text{P exp} \left\{ -ig \int dx_\mu A^\mu \right\}. \quad (2.5)$$

The integration contour runs from $-\infty$ to $+\infty$ close to the light cone with the “angle” defined by rapidity Y and A^μ being the gluon field of the target. The trace in Eq. (2.4) is in the fundamental representation. In perturbative LLA, in the absence of a target one has $A^\mu = 0$, leading to $U = 1$, $W = N_c$ giving $S = 1$ and $N = 0$, indicating zero interaction cross section as expected. In the opposite limit of very strong interactions one should get the black disk limit, which corresponds to $N = 1$ and $S = 0$ [17]. Hence $0 \leq N, S \leq 1$.

The QCD scattering problem as formulated by Eqs. (2.2), (2.3) and (2.1) and shown in Fig. 1 can be easily generalized to $\mathcal{N} = 4$ SYM theories at strong coupling by means of the AdS/CFT prescription outlined in [62, 63] (for a review see [65]). Following [62], we represent the quark and the anti-quark in the $\mathcal{N} = 4$ SYM theory as W-bosons coming from the breaking $U(N_c + 1) \rightarrow U(N_c) \times U(1)$. Our “quarks” are going to be very massive and would not recoil when interacting with the nucleus, thus justifying the Wilson loop approximation for the forward scattering amplitude.* The gravity dual description of the $\mathcal{N} = 4$ SYM $q\bar{q}$ dipole corresponds to an open string in the AdS_5 space whose endpoints, the quark and the anti-quark, are located at the boundary of the AdS_5 space. Parameterizing the two-dimensional world sheet of the string by the coordinates (τ, σ) , the location of the string in the five-dimensional world is given by

$$X^\mu = X^\mu(\tau, \sigma), \quad \mu = 0, \dots, 4. \quad (2.6)$$

The string’s Nambu-Goto action is

$$S_{NG} = \frac{1}{2\pi\alpha'} \int d\tau d\sigma \sqrt{-\det G_{\alpha\beta}} \quad (2.7)$$

with

$$G_{\alpha\beta} = g_{\mu\nu}(X) \partial_\alpha X^\mu \partial_\beta X^\nu, \quad \alpha, \beta = \sigma, \tau, \quad (2.8)$$

*While the infinite mass of the “quarks” justifies the recoilless approximation for their interaction with the target, the question arises of applicability of this model to the description of real DIS processes with light quarks, which indeed recoil during the interaction. For instance, while at small coupling in the leading logarithmic $\alpha_s \ln 1/x_{Bj}$ approximation the recoilless approximation is justified [19, 21, 17, 18], its validity becomes less clear at the subleading logarithmic order (order $\alpha_s^2 \ln 1/x_{Bj}$) [39]. We note that the recoil of the quarks at high energy only affects the impact factors (see e.g. [84]), and not the part of the interaction described by the small- x_{Bj} evolution. Thus the calculation below, when applied to light quarks, should be understood as calculation of the evolution without the impact factors. While the impact factors are likely to be numerically important, we will proceed under the assumption that they will not affect the qualitative features of the obtained scattering amplitude.

where $g_{\mu\nu}$ will be taken below to be the metric of the AdS_5 space in the presence of the shock wave and α' is the slope parameter. The AdS/CFT correspondence prescription of [62] dictates that in the limit of large 't Hooft coupling

$$\lambda = g_{YM}^2 N_c \quad (2.9)$$

with g_{YM} the Yang-Mills coupling constant, and in the large- N_c limit, the expectation value of the Wilson loop is given by the classical Nambu-Goto action of the open string in AdS_5 space

$$\langle W_{\mathcal{C}} \rangle \sim e^{iS_{NG}}, \quad (2.10)$$

where \mathcal{C} represents the closed contour spanned by the quark and the anti-quark at the string endpoints.

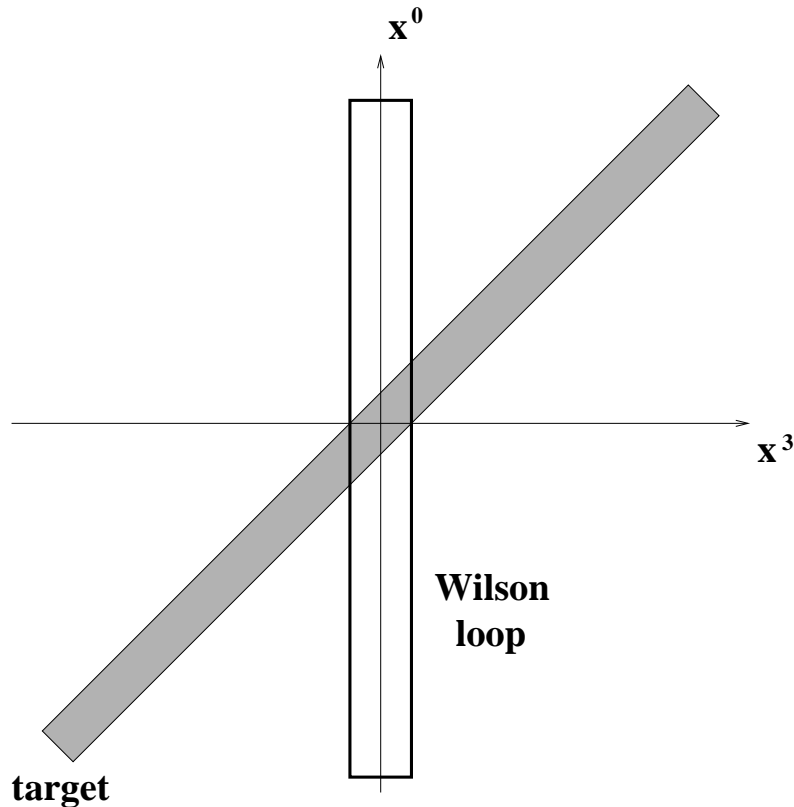


Figure 2: The same DIS process as in Fig. 1, only viewed in the rest frame of the dipole, as considered in the text. Separation of the quark and the anti-quark lines in x^3 direction was put in the figure only to guide the eye: in the text both the quark and the anti-quark are located at the same x^3 .

To complete the gravity dual description of the DIS scattering process we still have to determine the metric of the AdS_5 space in the presence of the nucleus. To that end we first introduce light-cone

coordinates

$$x^\pm = \frac{x^0 \pm x^3}{\sqrt{2}} \quad (2.11)$$

with x^0 the time direction. Following Janik and Peschanski [85], we consider the ultra-relativistic nucleus as a shock wave moving along the positive x^3 direction with its energy momentum tensor given by

$$\langle T_{--} \rangle = \frac{N_c^2}{2\pi^2} \mu \delta(x^-), \quad (2.12)$$

with all the other components being equal to zero. The physical interpretation of the scale μ , that has dimensions of mass cubed, and of the factor N_c^2 in Eq. (2.12) will be discussed below. Then, according to holographic renormalization [86], and using Fefferman-Graham coordinates [87], the gravity dual description of the CFT energy-momentum tensor in Eq. (2.12) is given by the following line element

$$ds^2 = \frac{L^2}{z^2} [-2 dx^+ dx^- + \mu \delta(x^-) z^4 dx^{-2} + dx_\perp^2 + dz^2], \quad (2.13)$$

where $dx_\perp^2 = (dx^1)^2 + (dx^2)^2$ with x^1 and x^2 being the coordinates transverse to the direction of motion of the nucleus, z is the coordinate describing the 5th dimension and L is the curvature radius of the AdS_5 space. In these coordinates the boundary of the AdS_5 space, and therefore the endpoints of the string representing the dipole, is at $z = 0$.

From now on we will work in the $q\bar{q}$ dipole's rest frame. There the Wilson loop in Eq. (2.3) becomes time-like, as shown in Fig. 2. We choose the dipole orientation to be parallel to the plane of the shock wave. We believe such configuration is the most relevant for studying DIS. Our choice of coordinates is such that the quark and anti-quark are located at $x^2 = x^3 = z = 0$ and $x_1 = \pm r/2$ respectively, with r the dipole's transverse size. We recall that, due to the eikonal approximation, the quark and the anti-quark remain fixed at those spatial locations throughout the collision process, thereby providing the appropriate Dirichlet boundary conditions for the string motion. Therefore, we find it convenient to parametrize the string coordinates (2.6) in terms of the proper time in the dipole rest frame, t , and $x^1 \equiv x$ in the following way:

$$\tau = t, \quad \sigma = x \in \left[-\frac{r}{2}, \frac{r}{2}\right], \quad (2.14)$$

$$X^\mu(\tau, \sigma) \rightarrow (X^0 = t, X^1 = x, X^2 = 0, X^3 = 0, X^4 = z(t, x)). \quad (2.15)$$

We note that the symmetries of the problem allow us to set $X^2 = 0$ for all times, since nothing in the problem depends on x^2 . Analogous symmetry arguments indicate that the string coordinate along the collision axis, X^3 , is equal to zero *before* the collision with the target. A priori, there is no

dynamical argument allowing us to set $X^3 = 0$ at all times. Indeed, the shock wave metric (2.13) is strongly singular at $t = x^3$ and, therefore, it is conceivable that after being hit by the nucleus the string develops some kind of motion in x^3 -direction, such as recoil or oscillation. However, it can be proven that for the particular dynamical limit that we are interested here, namely in the static limit that we shall discuss in detail in Section 3, the dynamics of the X_3 component of the string coordinates is trivial, allowing us to set it to a constant value, which we choose here to be equal to zero. In the general time-dependent case we would not expect X^3 to be equal to zero. The collision process as described in the previous paragraphs is represented in Fig. 2.

Before proceeding any further let us pause to interpret our choices Eq. (2.12) and Eq. (2.13), which provide the embedding of the ultra-relativistic nucleus into the AdS_5 space. First of all, as it was shown in [85], the shock wave metric in Eq. (2.13) is an exact solution of the Einstein equations in five dimensions with negative cosmological constant $\Lambda_c = -6/L^2$, and, therefore, provides a plausible gravity representation of an ultra-relativistic nucleus. Secondly, let us relate the parameter μ in Eq. (2.12) to some physical quantities. The energy-momentum tensor in Eq. (2.12) corresponds to a nucleus made out of many massless ultra-relativistic point particles. Thus, we envision the nucleus as a set of A nucleons, each of them consisting of N_c^2 *valence* point-like charges moving with light-cone momentum p^+ along the positive x^+ direction. In our model the nucleus is infinite and homogeneous in the (x^1, x^2) -plane transverse to its direction of motion (x^3). The energy-momentum tensor of an ultra-relativistic point particle moving with momentum p^+ along the light cone at transverse position \mathbf{y} and at the other light cone coordinate $x^- = 0$ is $T_{--}(x) = p^+ \delta^2(\mathbf{x} - \mathbf{y}) \delta(x^-)$. Summing over N_c^2 gluons in each nucleon and over all A nucleons in the nucleus and averaging over transverse coordinates \mathbf{y} we write

$$\langle T_{--}^{nucleus} \rangle = \frac{A N_c^2}{S_{\perp}} \int d^2 y p^+ \delta^2(\mathbf{x} - \mathbf{y}) \delta(x^-) = \frac{A N_c^2}{S_{\perp}} p^+ \delta(x^-) = \frac{N_c^2}{2\pi^2} A^{1/3} \Lambda^2 p^+ \delta(x^-) \quad (2.16)$$

where $S_{\perp} \approx A^{2/3} \pi R_N^2$ is the transverse area of the nucleus, R_N is the nucleon radius and $\Lambda^2 = 2\pi^2/\pi R_N^2$ is a characteristic transverse momentum scale. Comparing Eqs. (2.12) and (2.16) one can now identify the scale μ in Eq. (2.12) in terms of the physical scales characterizing the nucleus

$$\mu = p^+ \Lambda^2 A^{1/3}. \quad (2.17)$$

It is worth noting that if we had not assumed the existence of N_c^2 *valence* particles per nucleon, then the perturbation to the metric of the empty AdS_5 space due to the presence of the nucleus would be suppressed by a factor of $1/N_c^2$, becoming negligible in the strict $N_c \rightarrow \infty$ limit.

Eq. (2.17) will serve as our expression for μ . A more general treatment for the energy-momentum tensor of a nucleus in the context of high-energy scattering has been recently proposed by the authors in [88]. In particular one could argue that the energy-momentum tensor of the nucleus at large coupling should not be limited to only the valence quarks (gluons) contribution. The strong gluon fields should also contribute to the energy-momentum tensor, and their contribution is likely

to be dominant at large coupling. The energy-momentum tensor of such fields is fixed by conformal invariance of $\mathcal{N} = 4$ SYM theory at hand. The structure of the energy-momentum tensor is the same as in an Abelian theory: it was calculated in Appendix A of [88]. Here we will simply argue that such energy-momentum tensor could be approximated by Eq. (2.12) with μ given by Eq. (2.17) times a factor of $\sqrt{\lambda}$. Such tensor would not qualitatively change our discussion below, but it will modify the expression (2.17) for μ that we will use in what follows.

Under the approximation of a homogeneous nucleus having an infinite transverse extent the nuclear energy-momentum tensor is independent of the transverse coordinates, as reflected in Eq. (2.12). This means that all the relevant dynamical quantities become rotationally invariant and independent on the impact parameter of the collision, depending only on the dipole size, $r = |\mathbf{r}|$, and on the collision energy:

$$W(\mathbf{x}, \mathbf{y}, Y) \rightarrow W(r, Y), \quad N(\mathbf{r}, \mathbf{b}, Y) \rightarrow N(r, Y), \quad S(\mathbf{r}, \mathbf{b}, Y) \rightarrow S(r, Y). \quad (2.18)$$

Let us generalize the perturbative formulation of the scattering problem in Eq. (2.3) to the large coupling case. Using Eqs. (2.2), (2.3) and (2.10) we write

$$S(r, Y) = \text{Re} \left[\frac{\langle W \rangle_\mu}{\langle W \rangle_{\mu \rightarrow 0}} \right] = \text{Re} \left[e^{i[S_{NG}(\mu) - S_{NG}(\mu \rightarrow 0)]} \right] \quad (2.19)$$

and

$$N(r, Y) = 1 - S(r, Y). \quad (2.20)$$

In Eq. (2.19) $\langle W \rangle_\mu$ is the static Wilson loop pictured in Fig. 2 and $S_{NG}(\mu)$ is the corresponding classical Nambu-Goto action of the open string evaluated in the background of the shock wave. $\langle W \rangle_{\mu \rightarrow 0}$ and $S_{NG}(\mu \rightarrow 0)$ are the same quantities in the limit of $\mu \rightarrow 0$. Dividing by $\langle W \rangle_{\mu \rightarrow 0}$ in Eq. (2.19) insures that we remove the contribution to the Wilson loop *not* generated by the interaction with the shock wave [52].

3. Static Solution

As we discussed in the previous section, the calculation of the DIS cross-section at strong coupling under the AdS/CFT correspondence reduces to finding the classical trajectory of the string in the background of the shock-wave metric in Eq. (2.13). However, finding the time-dependent analytic solution to the Euler-Lagrange equations associated with the Nambu-Goto action in Eq. (2.7) in the background of the metric (2.13) is a very difficult mathematical problem. In this section we concentrate in a somewhat simplified problem, the static limit, which we expect to be a good approximation for DIS on a very large nucleus.

Following the standard procedures used in perturbative calculations [6, 8, 25] we begin by relaxing the ultra-relativistic limit, allowing the nucleus to have a finite longitudinal extent in the x^- direction. This can be managed by “smearing” the delta function in Eq. (2.12):

$$\langle T_{--} \rangle = \frac{N_c^2}{2\pi^2} \mu \delta(x^-) \longrightarrow \frac{N_c^2}{2\pi^2} \frac{\mu}{a} \theta(x^-) \theta(a - x^-), \quad (3.1)$$

where θ is the Heaviside step function and

$$a \approx 2R \frac{\Lambda}{p^+} \sim \frac{A^{1/3}}{p^+} \quad (3.2)$$

is the width of the nucleus as seen from the dipole rest frame. (R is the radius of the nucleus.) After the replacement in Eq. (3.1) the shock wave metric in Eq. (2.13) has to be modified accordingly, getting

$$ds^2 = \frac{L^2}{z^2} \left[-2 dx^+ dx^- + \frac{\mu}{a} \theta(x^-) \theta(a - x^-) z^4 dx^{-2} + dx_\perp^2 + dz^2 \right]. \quad (3.3)$$

Recalling that we considered the string to be located at $x^3 = 0$, Eqs. (3.1) and (3.3) permit the following neat description of the temporal sequence of the collision. For $t < 0$ there is no interaction between the string and the nucleus and the string lives in the empty AdS_5 space. At $t = 0$ the string is hit by the front end of the nucleus. The interaction between the nucleus and the string continues until $t = a\sqrt{2}$. At that time the nucleus has completely passed through the string, which returns to the empty AdS_5 space. We now concentrate on times $t > 0$. We will assume that the string reaches a stationary time-independent configuration in a short excitation time t_e after being hit by the nucleus. Under that assumption, the string will remain in such stationary configuration during the remaining interaction time, i.e for $t_e < t < a\sqrt{2}$. Finally, at $t > a\sqrt{2}$ the interaction ceases and the string is likely to return to its original vacuum configuration after a given relaxation time, t_r . Very schematically, the contribution to the string action due to the interaction with the nucleus,

$$S_{NG}^I = S_{NG}(\mu) - S_{NG}(0), \quad (3.4)$$

can be written as

$$S_{NG}^I = \left\{ \int_0^{t_e} dt + \int_{t_e}^{a\sqrt{2}} dt + \int_{a\sqrt{2}}^{a\sqrt{2}+t_r} dt \right\} \int dx \mathcal{L} \quad (3.5)$$

where \mathcal{L} is the Lagrangian density. Under the additional assumption that both the transition and relaxation times are much smaller than the nuclear width, i.e. that

$$a \gg t_e \sim t_r, \quad (3.6)$$

one can conclude that S_{NG}^I is dominated by the contribution of the static, time-independent solution (the second term in the r.h.s of Eq. (3.5)). Unfortunately, we were not able to find a reliable parametric estimate of neither t_e nor t_s in terms of the dimensionful scales of the problem, μ and a .

Instead we notice that, as can be checked explicitly, the time-dependent equations of motion for a string right after the nucleus hit it (and right after the string leaves the nucleus) depend only on the ratio μ/a and on the boundary conditions at $x = \pm r/2$, i.e., on r . (As we will see soon, the same applies to the static string equations of motion inside the shock wave, which do not “know” about the length of the shock wave.) As neither μ/a nor r depend on A (see Eqs. (2.17) and (3.2)), we conclude that t_e and t_r , along with the Nambu-Goto action for the string, are independent of A . Hence the second integral on the right hand side of Eq. (3.5) is the only A -dependent term in Eq. (3.5) and, as it grows with A , it is bound to dominate at large enough A . Therefore, in the limit of very large nucleus the static approximation will be justified.

One could also justify the static approximation in a different way by slightly changing the physical problem. One could imagine that in DIS the virtual photon enters the shock wave, and then fluctuates into the $q\bar{q}$ pair. The $q\bar{q}$ pair travels through the shock wave, and, for the forward amplitude, it would quickly recombine back into a virtual photon before leaving the shock wave. Interaction of such a dipole with the shock wave has to be static, as the dipole would not “know” about the ends of the shock wave. Integrating over the possible splitting and recombination times would yield Eqs. (2.20) and (2.19).

In the static limit corresponding to scattering on a very large nucleus as described above all the relevant dynamical quantities become independent of time. We take the smeared large nucleus with the energy-momentum tensor described in Eq. (3.1). The metric corresponding to such shock wave is given in Eq. (3.3). To achieve the static limit one has to remove the product of theta-functions in Eq. (3.3). Changing from light-cone coordinates to (t, x^3) coordinates and dropping the theta-functions in Eq. (3.3) we obtain

$$ds^2 = \frac{L^2}{z^2} \left[- \left(1 - \frac{\mu}{2a} z^4 \right) dt^2 + \left(1 + \frac{\mu}{2a} z^4 \right) (dx^3)^2 - \frac{\mu}{a} z^4 dt dx^3 + (dx^1)^2 + (dx^2)^2 + dz^2 \right]. \quad (3.7)$$

Let us note that the shock wave metric in Eq. (3.7), just like the metrics in Eqs. (2.13) and (3.3), is an exact solution of the Einstein equations in empty AdS₅ space

$$R_{\mu\nu} + \frac{4}{L^2} g_{\mu\nu} = 0. \quad (3.8)$$

On the gauge theory side the metric in Eq. (3.7) corresponds to a uniform shock wave with an infinite longitudinal and transverse extent and with the only non-zero component of the energy-momentum tensor given by $\langle T_{--} \rangle = \frac{N_c^2}{2\pi^2} \frac{\mu}{a}$.

Substituting the static metric Eq. (3.7) into the Nambu-Goto action (2.7) and making use of the relation between the AdS₅ curvature radius L , the slope parameter α' and the string coupling

$\sqrt{\lambda}$

$$\frac{L^2}{\alpha'} = \sqrt{\lambda} \quad (3.9)$$

yields

$$S_{NG}(\mu) = \int_0^{a\sqrt{2}} dt \int_{-r/2}^{r/2} dx \mathcal{L}^{static}, \quad (3.10)$$

where

$$\mathcal{L}^{static} = \frac{\sqrt{\lambda}}{2\pi} \frac{1}{z^2} \sqrt{(1+z'^2) \left(1 - \frac{\mu}{2a} z^4\right)} \quad (3.11)$$

is the static Lagrangian density. $z \equiv z(x)$ is the string coordinate along the 5th dimension of the AdS₅ space (henceforth we shall drop the argument of z). The prime in Eq. (3.11) denotes a derivative with respect to x .

We now have all the necessary ingredients to proceed to the calculation of the classical string configuration in the static limit. Before doing we note that

$$\frac{\mu}{2a} \approx \frac{1}{2} p^{+2} \Lambda^2. \quad (3.12)$$

The center of mass energy s of the collision is proportional to the product of p^+ and some scale characterizing the dipole. Indeed our dipole is made out of heavy quarks with large mass M , so it may appear natural to put $s \sim p^+ M$. However, later on we will renormalize the Nambu-Goto action that we will obtain by subtracting its contribution to the quark mass. Hence we will effectively remove M out of the problem. Hence the center of mass energy of the dipole would be equal to p^+ times some transverse momentum scale characterizing the dipole. We will put the latter scale to be proportional to the scale Λ of the nucleus, such that $s \sim p^+ \Lambda$. We thus “define”

$$\frac{\mu}{2a} = s^2. \quad (3.13)$$

The Euler-Lagrange equation of motion associated with the Lagrangian Eq. (3.11) reads

$$\frac{\partial}{\partial x} \frac{\partial \mathcal{L}^{static}}{\partial z'} - \frac{\partial \mathcal{L}^{static}}{\partial z} = 0 \quad (3.14)$$

and straightforwardly leads to

$$z z'' (1 - s^2 z^4) + 2(z'^2 + 1) = 0. \quad (3.15)$$

We need to solve Eq. (3.15) with the boundary condition

$$z(x = \pm r/2) = 0 \quad (3.16)$$

which insures that the string ends at the boundary of the AdS₅ space.

Using $z'' = \frac{dz'}{dz} z'$, the first integral of Eq. (3.15) can be readily obtained. We get

$$z'^2 = \left(\frac{z_{max}}{z}\right)^4 \frac{1 - s^2 z^4}{1 - s^2 z_{max}^4} - 1, \quad (3.17)$$

where the constant of integration z_{max} has the meaning of the maximum extent of the string in the z -direction, since $z' = 0$ at $z = z_{max}$ (see Fig. 3). z_{max} is the fundamental parameter characterizing the static solution since, as we will show shortly, all the relevant physical quantities can be parametrized directly in terms of z_{max} .

As $dx = dz/z'$, we write

$$dx = \frac{dz}{\pm \sqrt{\left(\frac{z_{max}}{z}\right)^4 \frac{1 - s^2 z^4}{1 - s^2 z_{max}^4} - 1}}. \quad (3.18)$$

Picking the half of the string where $z' > 0$ we integrate over x from $-r/2$ to x and, using Eq. (3.16) obtain

$$x + \frac{r}{2} = \int_0^z \frac{d\tilde{z}}{\sqrt{\left(\frac{z_{max}}{\tilde{z}}\right)^4 \frac{1 - s^2 \tilde{z}^4}{1 - s^2 z_{max}^4} - 1}}. \quad (3.19)$$

Performing the integral in Eq. (3.19) yields

$$x + \frac{r}{2} = \frac{z^3}{3 z_{max}^3} z_{max} \sqrt{1 - s^2 z_{max}^4} F\left(\frac{1}{2}, \frac{3}{4}; \frac{7}{4}; \frac{z^4}{z_{max}^4}\right) \quad (3.20)$$

with F the hypergeometric function. The curve in Eq. (3.20) is sketched in Fig. 3.

From symmetry considerations z_{max} must lie at the midpoint between the two string endpoints, i.e. at $x = 0$. Putting $x = 0$ and $z = z_{max}$ in Eq. (3.20) yields the following relation between z_{max} , the collision energy \sqrt{s} and the dipole size r

$$c_0 r = z_{max} \sqrt{1 - s^2 z_{max}^4}, \quad (3.21)$$

where we have defined a constant

$$c_0 \equiv \frac{\Gamma^2\left(\frac{1}{4}\right)}{(2\pi)^{3/2}}. \quad (3.22)$$

The case considered by Maldacena in [62] for a static Wilson loop without a shock wave can be recovered from Eq. (3.21) by putting $s = 0$ in it, thus eliminating the shock wave. In that limit one gets $z_{max} = z_{max}^M \equiv c_0 r$.

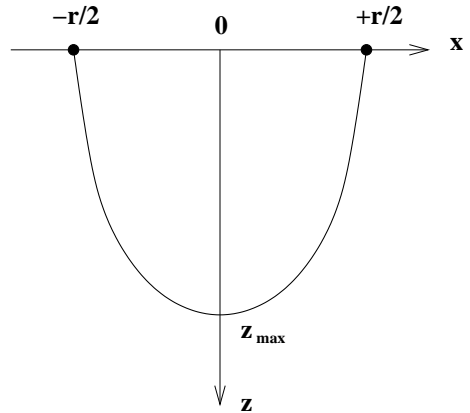


Figure 3: A sketch of the string configuration solving Eq. (3.15) and given by Eq. (3.23) in the (x, z) -plane.

Finally, with the help of Eq. (3.21), the classical solution for the open string in Eq. (3.20) becomes

$$x + \frac{r}{2} = \frac{z^3}{3 z_{max}^3} c_0 r F\left(\frac{1}{2}, \frac{3}{4}, \frac{7}{4}; \frac{z^4}{z_{max}^4}\right) \quad (3.23)$$

for $-(r/2) \leq x \leq 0$ with a mirror image obtained by replacing $x \rightarrow -x$ in Eq. (3.23) for $0 \leq x \leq r/2$.

4. Evaluating the S-matrix

We proceed by evaluating the Wilson loops in Eq. (2.19) using Eq. (2.10) with the classical string configurations found above. As we will see now, Eq. (3.21) relating the string maximum to the collision energy and the dipole size has three different complex-valued solutions. As we shall see below, each of the solutions leads to a different behavior of the DIS cross-section. It turns out that the physically meaningful solution can be obtained in two ways which are described below.

4.1 General Evaluation

We first study the solutions of Eq. (3.21) for the string maximum, z_{max} . Introducing the dimensionless parameters

$$\xi = \frac{z_{max}^2}{c_0^2 r^2}, \quad m = c_0^4 r^4 s^2, \quad (4.1)$$

Eq. (3.21) can be rewritten as the following cubic equation for ξ

$$m \xi^3 - \xi + 1 = 0. \quad (4.2)$$

Obviously, for $m \neq 0$ Eq. (4.2) has three different complex roots. Solving the cubic equation (4.2) we get

$$\xi = \frac{1}{3m\Delta} + \Delta, \quad (4.3)$$

with

$$\Delta = \left[-\frac{1}{2m} + \sqrt{\frac{1}{4m^2} - \frac{1}{27m^3}} \right]^{1/3} \exp\left[i \frac{2\pi n}{3} \right]. \quad (4.4)$$

The index n in Eq. (4.4) takes on values $n = 0, 1, 2$, corresponding to the three different Riemann sheets of the cubic root, and characterizes the three solutions of Eq. (4.2). From here on we will stick to the convention that the cubic root is evaluated by taking the principal branch, while all

the information distinguishing one branch from another will be shown explicitly in terms of n . Also one writes, using Eq. (4.1),

$$z_{max} = c_0 r \sqrt{\xi}, \quad (4.5)$$

where we agree to take the principal branch of the square root. (One can show that the secondary branch does not lead to any new physical solutions.) The branch cut for all roots is taken along the negative real axis.

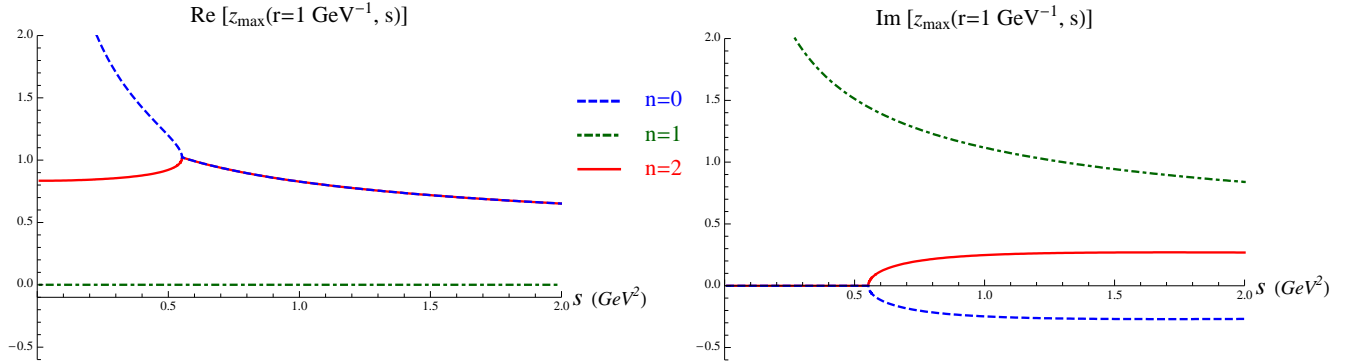


Figure 4: Real (left plot) and imaginary (right plot) parts of $z_{max}(r = 1 \text{ GeV}^{-1}, s)$ given by Eqs. (4.5), (4.4) and (4.3) plotted as a function of the collision energy s . The figure contains all three branches of the solution corresponding to $n = 0$ (dashed line), $n = 1$ (dot-dashed line) and $n = 2$ (solid line).

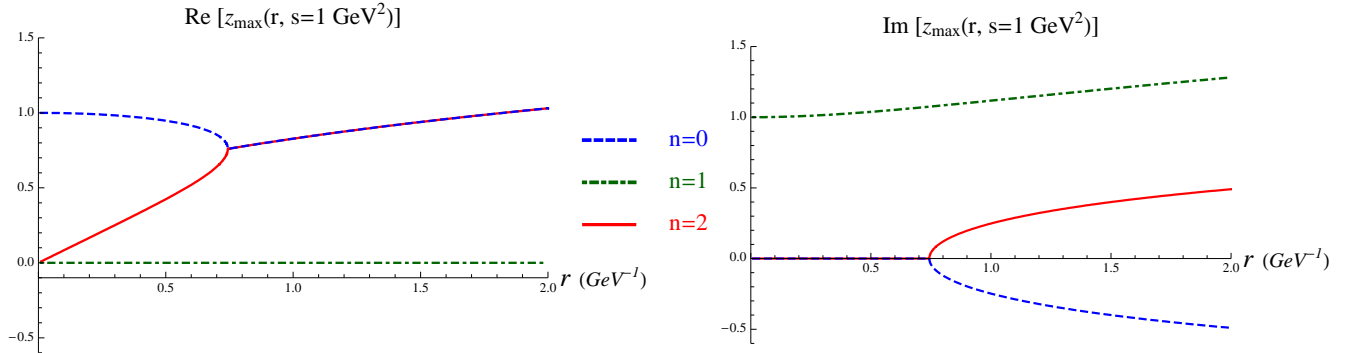


Figure 5: Real (left plot) and imaginary (right plot) parts of $z_{max}(r, s = 1 \text{ GeV}^2)$ given by Eqs. (4.5), (4.4) and (4.3) plotted as a function of the dipole size r . Again the three branches of the solution are $n = 0$ (dashed line), $n = 1$ (dot-dashed line) and $n = 2$ (solid line).

The three different z_{max} corresponding to the three solutions of Eq. (4.2) are shown in Figs. 4 and 5 as functions of energy s and the dipole transverse size r . As shown in Figs. 4 and 5, and as

can be demonstrated by an analytical calculation, one of the three solutions of Eq. (4.2), the one corresponding to $n = 1$, is purely imaginary while the other two, corresponding to $n = 0$ and $n = 2$, are real for small r and for small s , becoming complex and conjugate to each other for larger r and s once the condition of $m > 4/27$ is satisfied.

Complex-valued solutions like these arise in the quasi-classical approximations to quantum mechanics (see e.g. ch. 131 in [76]). They correspond to motion in the classically forbidden region. Our physical interpretation of the complex-valued string coordinates is that the string is classically prohibited from going through the shock wave: such motion can only happen quasi-classically. Another way of thinking about this result is to observe that the saddle-point corresponding to the classical approximation does not have to lie in the domain of real-valued string coordinates only, and can in general be complex-valued. For similar cases in AdS/CFT framework see [77].

In order to figure out which of the three branches leads to the right physical behavior of the dipole scattering amplitude we need to know the limiting behavior of z_{max} as $m \rightarrow 0$ and $m \rightarrow \infty$ respectively. A straightforward expansion of Eqs. (4.5), (4.4) and (4.3) yields

$$\lim_{m \rightarrow \infty} z_{max} = \left(\frac{c_0 r}{s}\right)^{1/3} \begin{cases} \exp[-i\frac{\pi}{6}], & \text{for } n = 0 \\ i, & \text{for } n = 1 \\ \exp[i\frac{\pi}{6}], & \text{for } n = 2 \end{cases} ; \quad \lim_{m \rightarrow 0} z_{max} = \begin{cases} 1/\sqrt{s}, & \text{for } n = 0 \\ i/\sqrt{s}, & \text{for } n = 1 \\ c_0 r, & \text{for } n = 2 \end{cases} . \quad (4.6)$$

From Eq. (4.6) one can see right away that only the $n = 2$ branch of the solution maps onto the Maldacena result from [62] in the limit of no shock wave, i.e. as $m \rightarrow 0$. One can also see this from Figs. 4 and 5. Thus if we were to require that the string coordinates map onto Maldacena's case for $m \rightarrow 0$, it would seem clear that one has to take the $n = 2$ branch of the solution. However, as we will see shortly, such branch does not give a unitary $N(r, Y)$ at large r : in fact $N(r, Y)$ becomes *negative* at large r for the $n = 2$ branch. Hence, to obtain a physically meaningful solution, we have to either abandon the requirement of mapping the string coordinate onto the Maldacena configuration [62], or allow for the string to “jump” from one branch to another. The two possibilities are explored below.

First let us calculate the Nambu-Goto action at the extremal solutions found above. Combining Eqs. (3.10) and (3.11) and using $dx = dz/z'$ we write

$$S_{NG}(\mu) = \frac{\sqrt{2\lambda} a}{\pi} \int_0^{z_{max}} \frac{dz}{z'} \frac{1}{z^2} \sqrt{(1+z'^2)(1-s^2 z^4)} \quad (4.7)$$

where the factor of 2 comes from adding the two halves of the string. Using Eq. (3.17) in Eq. (4.7) yields

$$S_{NG}(\mu) = \frac{\sqrt{2\lambda} a}{\pi} z_{max}^2 \int_0^{z_{max}} \frac{dz}{z^2} \frac{1-s^2 z^4}{\sqrt{z_{max}^4 - z^4}}. \quad (4.8)$$

The integral in Eq. (4.8) has an ultraviolet divergence at $z = 0$ due to infinite quark masses. To renormalize the result one has to subtract out the infinity [62] by removing contributions of individual quarks. The mass of a single quark in vacuum is calculated by attaching a straight-line string to the boundary of the AdS space, with the other end of the string going straight into the bulk. However, similar to the case of a heavy quark potential at finite temperature [65], it is not clear here whether we should also subtract such an infinite straight string configuration, or let the string end somewhere.

We would like to subtract out contributions of static straight open strings, “hanging” from the quark and the anti-quark into the AdS space stretching up to $z = +\infty$. However the shock wave metric in Eq. (3.7) appears to have an analogue of a horizon. Namely, for $z = z_h$ with the “horizon” defined by

$$z_h \equiv \frac{1}{\sqrt{s}} \quad (4.9)$$

the g_{tt} component of the metric becomes zero. Moreover, for $z > z_h$, no light-like trajectories along the z -axis (without moving in x^3 direction) are possible. Therefore the string world-sheet can not stretch into the $z > z_h$ region. The situation is analogous to the finite temperature calculations of heavy quark potential, where one subtracts the contributions of strings stretching up to the black hole horizon [63, 65]. Following [63, 65] we will subtract the straight-string configuration shown in Fig. 6 out of the action in Eq. (4.8). Our strings in Fig. 6 stretch only up to the horizon z_h . The action corresponding to two straight strings shown in Fig. 6 is obtained from Eq. (4.7) by taking $z' \rightarrow \infty$ limit in it and limiting the integration between $0 < z < z_h$. Thus we will subtract

$$\frac{\sqrt{2\lambda} a}{\pi} \int_0^{z_h} \frac{dz}{z^2} \sqrt{1 - s^2 z^4} \quad (4.10)$$

from the action of Eq. (4.8).

Subtracting Eq. (4.10) out of the action in Eq. (4.8) and integrating over z we obtain the renormalized action

$$S_{NG}^{ren}(\mu) = \frac{\sqrt{\lambda} a}{\pi c_0 \sqrt{2}} \left[\frac{c_0^2 r^2}{z_{max}^3} - \frac{2}{z_{max}} + \frac{2}{z_h} \right]. \quad (4.11)$$

The action (4.11), when substituted into Eqs. (2.20) and (2.19) would give us the scattering amplitude $N(r, Y)$.

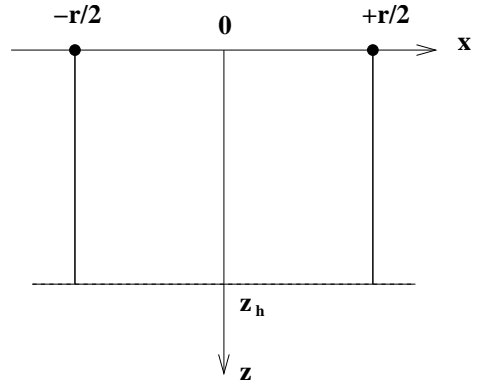


Figure 6: The string configuration which we subtract out to renormalize the Nambu-Goto action drawn in the (x, z) -plane. The dashed line indicates the horizon of the shock wave.

Knowing the action (4.11), and therefore the amplitude $N(r, Y)$, we can now see which ones of the three above solutions give physically meaningful $N(r, Y)$. Our criteria are simple: we want $N(r, Y) \rightarrow 0$ when $r \rightarrow 0$ (color transparency) and $N(r, Y) \rightarrow 1$ when $r \rightarrow \infty$ (the black disk limit). In addition $N(r, Y)$ should be positive-definite for $r > 0$, $N(r, Y)$ should be less than 1 at all r (unitarity) and $N(r, Y)$ should be a monotonically increasing function of r for all r .

A simple analysis using Eqs. (4.11), (2.19) and (2.19) rules out the $n = 2$ branch: as one can show, $N(r, Y)$ given by that branch becomes negative at large r . $n = 0$ branch appears to satisfy both the color transparency condition at small r and the black disk limit at large r . However, the amplitude $N(r, Y)$ on that branch is not a monotonic function and, more importantly, is not unitary: in a certain range of energies/dipole sizes it oscillates and could become greater than 1 violating unitarity. Hence this branch is also unphysical and should be discarded. This leaves us only with the $n = 1$ branch, which, as we will see shortly, gives a physically meaningful $N(r, Y)$.

The drawback of the $n = 1$ branch is that it does not map onto Maldacena's solution [62] in the $\mu \rightarrow 0$ limit. Requiring that such mapping takes place leaves us with the $n = 2$ branch, which is unphysical at large r . However, there is another possibility, which we will outline below. One can take a superposition of two branches for z_{max} : for small r (or s) one can use the $n = 2$ branch, while for larger r (or s) one can use the $n = 0$ branch. As the $n = 0$ and $n = 2$ branches of z_{max} intersect at $m = 4/27$, as can be seen from Figs. 4 and 5 and from Eq. (4.4), it is possible that a transition from one branch to another happens at this point. As we will also show below, to get a physical result from the superposition of the two branches one has to slightly modify the rule for calculating the contribution of the Wilson lines to the S -matrix (2.19). We will consider the single $n = 1$ branch solution first though.

4.2 Single Branch

As one can see from Eq. (4.6), and from a simple graphical analysis of Eq. (4.2), and also from Figs. 4 and 5, z_{max} given by the $n = 1$ branch of the solution is purely imaginary, with a positive imaginary part. As the coordinate x of the string is real, we infer from Eq. (3.23) that the complex phase of z should be the same as that of z_{max} . Therefore, for $n = 1$ branch z would be purely imaginary. Denote the positive imaginary part of z_{max} of $n = 1$ branch by ρ_{max} such that

$$z_{max}^{n=1} = i \rho_{max}, \quad \rho_{max} > 0. \quad (4.12)$$

Now, as z is purely imaginary, all z -integrals, including that in Eq. (4.10) should run along the positive imaginary axis. Therefore for the $n = 1$ branch we should replace $z_h \rightarrow i z_h$ in Eq. (4.11). We rewrite Eq. (4.11) as

$$S_{NG}^{ren}(\mu, n = 1) = i \frac{\sqrt{\lambda} a}{\pi c_0 \sqrt{2}} \left[\frac{c_0^2 r^2}{\rho_{max}^3} + \frac{2}{\rho_{max}} - \frac{2}{z_h} \right]. \quad (4.13)$$

As one can explicitly check $S_{NG}^{ren}(\mu \rightarrow 0, n = 1) = 0$. Using Eqs. (2.19) and (2.20) yields

$$N(r, s) = 1 - \exp \left\{ - \frac{\sqrt{\lambda} a}{\pi c_0 \sqrt{2}} \left[\frac{c_0^2 r^2}{\rho_{max}^3} + \frac{2}{\rho_{max}} - \frac{2}{z_h} \right] \right\}, \quad (4.14)$$

where we replaced $Y \sim \ln s$ with s in the argument of N .

As one can explicitly check $N(r, s)$ in Eq. (4.14) satisfies all physical criteria for a meaningful solution: it goes to zero as $r \rightarrow 0$, it approaches 1 as $r \rightarrow \infty$ and it varies monotonically in between, always staying positive for $r > 0$ and less than 1. The fact that the $N(r, s)$ in Eq. (4.14) is a monotonic function of r for all s is shown in detail in Appendix A.

Therefore, Eq. (4.14) is our answer for the forward scattering amplitude of a dipole on a nucleus given by the $n = 1$ branch. We will refer to it as Solution A. To find ρ_{max} one has to use Eqs. (4.12), (4.5), (4.4), (4.3) and (4.1) for $n = 1$, which can be summarized as follows:

$$\rho_{max} = -i r c_0 \sqrt{\frac{1}{3 m \Delta^{n=1}} + \Delta^{n=1}} \quad (4.15)$$

with

$$\Delta^{n=1} = \left[-\frac{1}{2m} + \sqrt{\frac{1}{4m^2} - \frac{1}{27m^3}} \right]^{1/3} \exp \left[i \frac{2\pi}{3} \right] \quad (4.16)$$

and $m = c_0^4 r^4 s^2$.

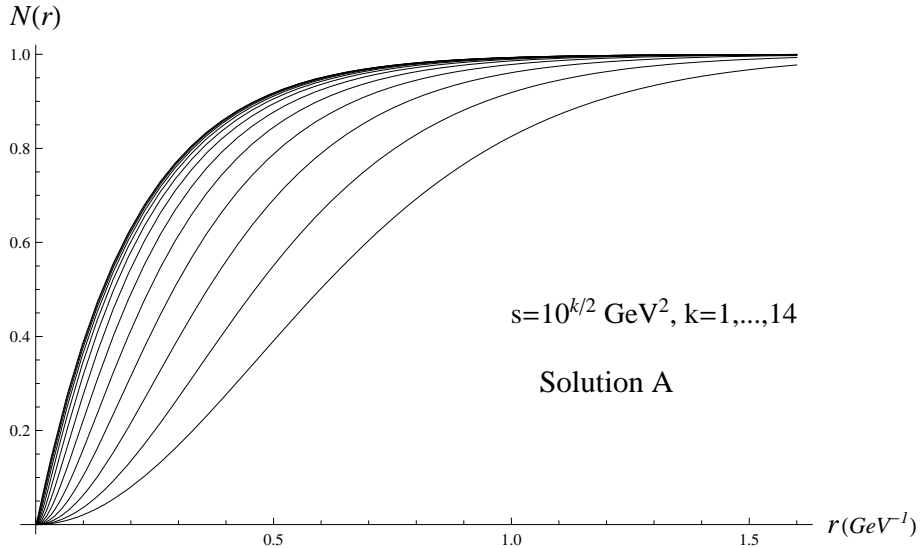


Figure 7: Dipole scattering amplitude $N(r, s)$ from Eq. (4.14) plotted as a function of the dipole size r for collision energies $s = 10^{k/2} \text{ GeV}^2$, $k = 1, \dots, 14$ (from right to left) with $\lambda = 20$, $A^{1/3} = 5$ and $\Lambda = 1 \text{ GeV}$.

$N(r, s)$ from Eq. (4.14) is plotted in Fig. 7 as a function of r for a range of center of mass energies s . According to Eq. (3.2) we put

$$a = A^{1/3} \frac{\Lambda}{s} \quad (4.17)$$

with $\Lambda = 1$ GeV. We also put $\lambda = 20$ and $A^{1/3} = 5$, which is not unrealistic for DIS on a gold nucleus. As one can see from Fig. 7, N increases with increasing energy, but the growth slows down as energy gets very high.

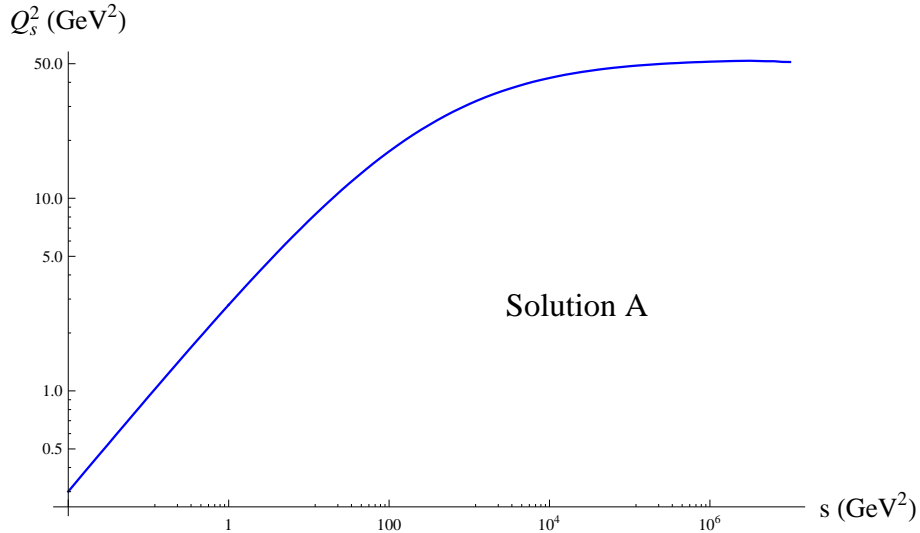


Figure 8: Saturation scale Q_s^2 as a function of the center-of-mass energy s corresponding to the same values of parameters as chosen for the solutions shown in Fig. 7. The saturation scale is obtained by imposing the condition $N(r = 1/Q_s, s) = 0.5$ on $N(r, s)$ in Eq. (4.14).

The saturation scale can be defined by requiring that $N(r = 1/Q_s, s) = 0.5$. It is plotted in Fig. 8 as a function of energy. The saturation scale also grows with energy, but at very high energy becomes a constant. It is interesting to note that fitting the region of linear growth of the logarithm of the saturation scale in Fig. 8 with a straight line one obtains

$$\ln \frac{Q_s^2}{\Lambda^2} \approx 0.9 + 0.47 \ln \frac{s}{\Lambda^2}. \quad (4.18)$$

However the growth stops approximately at $s \approx 100$ GeV² and $Q_s^2 \approx 20$ GeV² corresponding to $x_{Bj} \approx Q_s^2/s \approx 0.2$. For higher energies/smaller x_{Bj} the saturation scale is constant with energy/ x_{Bj} . This behavior is qualitatively similar to the "saturation of saturation" conjectured in [78] using very different (small coupling) physical arguments.

It would make more physical sense and facilitate the comparison to other approaches if we find the dependence of the forward amplitude $N(r, s)$ and of the saturation scale Q_s not only on s , but

also on x_{Bj} . The Bjorken- x variable in DIS is

$$x_{Bj} \equiv \frac{Q^2}{s + Q^2} \quad (4.19)$$

with Q^2 the virtuality of the photon. Replacing $Q \sim 1/r$ [79] we write

$$x_{Bj} \approx \frac{1}{1 + s r^2} \quad (4.20)$$

such that for $s r^2 \ll 1$

$$x_{Bj} \approx 1 - s r^2 \quad (4.21)$$

and for $s r^2 \gg 1$

$$x_{Bj} \approx \frac{1}{s r^2}. \quad (4.22)$$

To better understand our results in Eq. (4.14) and in Figs. 7 and 8, let us study the asymptotics of $N(r, s)$. At lower energies s and/or for smaller dipole sizes r we use the small- m asymptotics (see Eqs. (4.1) and (4.6)) of the solution to write

$$N(r, s) \Big|_{r^2 s \ll 1} = 1 - \exp \left\{ - \frac{\sqrt{\lambda} c_0}{2 \pi \sqrt{2}} r^2 s^{1/2} \Lambda A^{1/3} \right\}. \quad (4.23)$$

Note that in this limit $x_{Bj} \approx 1 - s r^2 = o(1)$ and the conclusions derived from Eq. (4.23) will not apply to small- x_{Bj} physics. The low- s and low- r asymptotics of the dipole is certainly energy-dependent, as can also be seen from Fig. 7. One can use Eq. (4.23) to extract the saturation scale: requiring that at $r = 1/Q_s$ the power of the exponent is approximately of order 1 yields

$$Q_s^2 \sim \sqrt{s} \Lambda A^{1/3} \sqrt{\lambda}, \quad m \ll 1, \quad (4.24)$$

in agreement with the fit (4.18) of Fig. 8 and the result of [60].

However, as $m \approx s^2 r^4$, the condition of $m \ll 1$ means that $s r^2 \ll 1$. We see that Eq. (4.23) is valid only for large x_{Bj} . Rewriting Eq. (4.23) in terms of r and x_{Bj} then yields

$$N(r, s) \Big|_{r^2 s \ll 1} = 1 - \exp \left\{ - \frac{\sqrt{\lambda} c_0}{2 \pi \sqrt{2}} r \sqrt{1 - x_{Bj}} \Lambda A^{1/3} \right\}. \quad (4.25)$$

We see now that as a function of x_{Bj} the saturation scale is

$$Q_s \sim \sqrt{1 - x_{Bj}} \Lambda A^{1/3} \sqrt{\lambda}, \quad x_{Bj} \lesssim 1. \quad (4.26)$$

The expression for the saturation scale in Eq. (4.26) is valid at large (order 1) x_{Bj} only.

At high energy and/or large dipole sizes corresponding to the small- x_{Bj} limit, Eq. (4.14) in the $m \gg 1$ asymptotics gives

$$N(r, s) \Big|_{r^2 s \gg 1} = 1 - \exp \left\{ - \frac{\sqrt{\lambda}}{\pi \sqrt{2}} r \Lambda A^{1/3} \right\}. \quad (4.27)$$

Now $x_{Bj} \approx 1/(r^2 s) \ll 1$ (as $s r^2 \gg 1$) and we are in the small- x_{Bj} regime. The saturation scale can again be defined by requiring the power of the exponent to be of order 1. One then gets

$$Q_s \sim \sqrt{\lambda} \Lambda A^{1/3}. \quad (4.28)$$

The saturation scale is independent of energy s at high energies, in agreement with Fig. 8! It is also independent of x_{Bj} at small x_{Bj} . The saturation scale grows with the atomic number of the nucleus A as $Q_s \sim A^{1/3}$, which is a stronger growth than the perturbative QCD estimate of $Q_s \sim A^{1/6}$. The $Q_s \sim A^{1/3}$ scaling was also observed in [60], though for the saturation scale more similar to the one given by our Eq. (4.24). The saturation scale similar to our Eq. (4.28) was found in [89]. Finally we note that, while in both Eqs. (4.26) and (4.28) the saturation scale grows proportional to $\sqrt{\lambda}$ at fixed x_{Bj} , the exact power of λ depends on the energy-momentum of the shock wave used. As we have already mentioned above, the energy-momentum tensor of the gluon field at strong coupling has an extra power of $\sqrt{\lambda}$ as compared to the energy-momentum tensor of the valence gluons (3.1) that we used above. Using the energy-momentum tensor of the gluon field in the shock wave metric would modify the powers of λ in the above expressions for the saturation scales. In particular Eq. (4.28) would then be modified to give $Q_s \sim \lambda^{3/4}$.

Let us stress that, while the solution presented in this Subsection and given by Eq. (4.14) is one of the two possible physical solutions for $N(r, s)$, we believe that this solution is actually the correct one. As we will see below, the amplitude $N(r, s)$ given by the $n = 1$ branch does not have discontinuous r -derivative, unlike $N(r, s)$ given by the superposition of the other two branches. However, we do not have a solid physical argument to select the $n = 1$ solution over the other one.

4.3 Superposition of Two Branches

It is important to note that to derive our above result given by Eq. (4.14) we had to abandon the condition that the string coordinates map smoothly back onto Maldacena's vacuum solution [62] when $\mu \rightarrow 0$. Indeed the only branch of our solution satisfying such a condition, the $n = 2$ branch, would give a physically meaningless negative $N(r, s)$ at large r . However, if one insists on smooth matching with the vacuum string configuration of [62], one can construct a physically meaningful amplitude $N(r, s)$ using a superposition of two branches: one can use the $n = 2$ branch of the solution given by Eqs. (4.3), (4.1) and (4.4) for $m < 4/27$ and the $n = 0$ branch for $m > 4/27$. One can see from Eqs. (4.3), (4.1) and (4.4) that the values of z_{max} given by those two branches are equal at $m = 4/27$, which insures smooth matching of the values of the Nambu-Goto action

between the two solutions. (The fact that the two branches intersect can also be seen in Figs. 4 and 5.)

There is a subtlety here though. If one uses the Nambu-Goto action from Eq. (4.11) for the superposition of $n = 2$ and $n = 0$ branches along with Eqs. (2.19) and (2.20) to find $N(r, s)$, the resulting amplitude $N(r, s)$ would still not be physical. In fact, in a range of values for s and r it still has oscillations, which make $N(r, s)$ go above 1 and violate unitarity. These are the same oscillations that we have mentioned for the $n = 0$ branch above. The origin of such oscillations is in the fact that z_{max} for the $n = 0$ branch has a non-zero real part (see Figs. 4 and 5), leading to a non-zero real part for the Nambu-Goto action, which, when substituted into Eq. (2.19) gives cosine-like oscillations. However, such oscillations can be removed by modifying the prescription for the calculation of the S -matrix in Eq. (2.19). One can replace Eq. (2.19) with

$$S(r, Y) = e^{-\text{Im}[S_{NG}(\mu) - S_{NG}(\mu \rightarrow 0)]}. \quad (4.29)$$

Indeed by explicitly keeping the imaginary part of the Nambu-Goto action in the exponent, as shown in Eq. (4.29), we would get rid of the real part and, therefore, of the oscillations described above. Also, the new prescription in Eq. (4.29) would not change our above conclusions in Sect. 4.2 as the action of the $n = 1$ branch is purely imaginary. However, we do not have a good physical justification of Eq. (4.29) in general. In the quasi-classical approximation to quantum mechanics one usually takes only the imaginary part of the action to estimate scattering amplitudes along the complex quasi-classical trajectories, as could be seen from Eq. (131.14) in [76]. Hence our prescription (4.29) here is motivated by quantum mechanics and by the fact that it gives physically meaningful results here. It may be that for calculating the S -matrices, the prescription of [62], which was originally proposed for heavy quark potentials, has to be modified to that of Eq. (4.29).

Substituting Eq. (4.11) into Eq. (4.29), and using Eq. (2.20) yields

$$N(r, s) = 1 - \exp \left\{ -\frac{\sqrt{\lambda} a}{\pi c_0 \sqrt{2}} \text{Im} \left[\frac{c_0^2 r^2}{z_{max}^3} - \frac{2}{z_{max}} + \frac{2|z_{max}|}{z_h z_{max}} \right] \right\}, \quad (4.30)$$

where we have modified the $2/z_h$ term in the square brackets to reflect the fact that the complex phase of z_h (and of all other z 's) should be the same as the complex phase of z_{max} , as follows from Eq. (3.23) and as we have noticed and used above in Sect. 4.2. z_h is still given by Eq. (4.9) above.

Eq. (4.30) is the main result of this section. We will refer to it as Solution B. When using it one should take z_{max} from the $n = 2$ branch of Eqs. (4.1), (4.3) and (4.4) for $m < 4/27$ and from the $n = 0$ branch of the same equations for $m > 4/27$. One can also notice that z_{max} from both $n = 2$ and $n = 0$ branches is purely real for $m < 4/27$ (see Figs. 4 and 5). Hence in practice Eq. (4.30) can be used with the $n = 0$ branch of z_{max} for all m . This would eliminate the need for quantum corrections to justify the transition between the branches. However, the $n = 0$ branch does not map onto Maldacena's vacuum solution [62]: hence by keeping $n = 0$ branch only we would also lose some of the justification for searching for solutions beyond the $n = 1$ branch described above.

Let us also note that, since z_{max} and, therefore, the string coordinates for this solution are real for $m < 4/27$ and become complex for $m > 4/27$, one can interpret $m = 4/27$ as the point when, in a purely classical sense, the string would break due to high energy of the shock wave. This interpretation is similar to the finite temperature case [63, 67].

The amplitude in Eq. (4.30) is plotted in Fig. 9 for the same set of parameters as the amplitude in Fig. 7. The striking feature of the amplitude in Fig. 9 is that $N(r, s) = 0$ for a range of non-zero

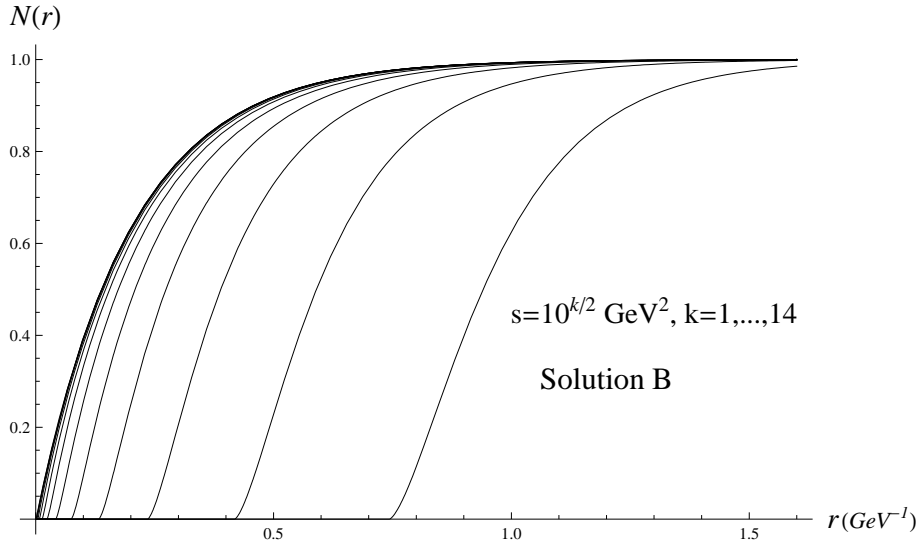


Figure 9: Dipole scattering amplitude $N(r, s)$ from Eq. (4.30) plotted as a function of the dipole size r for collision energies $s = 10^{k/2} \text{ GeV}^2$, $k = 1, \dots, 14$ (from right to left) with $\lambda = 20$, $A^{1/3} = 5$ and $\Lambda = 1 \text{ GeV}$.

values of r . This means that non-zero transverse size $q\bar{q}$ dipoles below certain critical transverse size would not interact with the shock wave. While such behavior appears somewhat unphysical, one may interpret it by arguing that at large coupling most partons are located at small- x_{Bj} . As small r corresponds to large x_{Bj} (see Eq. (4.20)), the small-size dipole does not resolve any partons, and thus does not interact. The exponential suppression of high- Q^2 (small- r) partons has been noticed before in [54, 53, 61, 60, 89]. Such exponential suppression possibly translates into 0 in our case.

Eq. (4.30) can be used to find the saturation scale by requiring again that $N(r = 1/Q_s, s) = 0.5$. It is plotted in Fig. 10 as a function of energy. Similar to the $n = 1$ branch in Fig. 8, the saturation scale also grows with energy, but at very high energy becomes a constant. Fitting the growing part of the curve in Fig. 10 with a straight line yields

$$\ln \frac{Q_s^2}{\Lambda^2} \approx 0.25 + 0.95 \ln \frac{s}{\Lambda^2}. \quad (4.31)$$

Again the growth of the saturation scale stops at a rather large values of x_{Bj} .

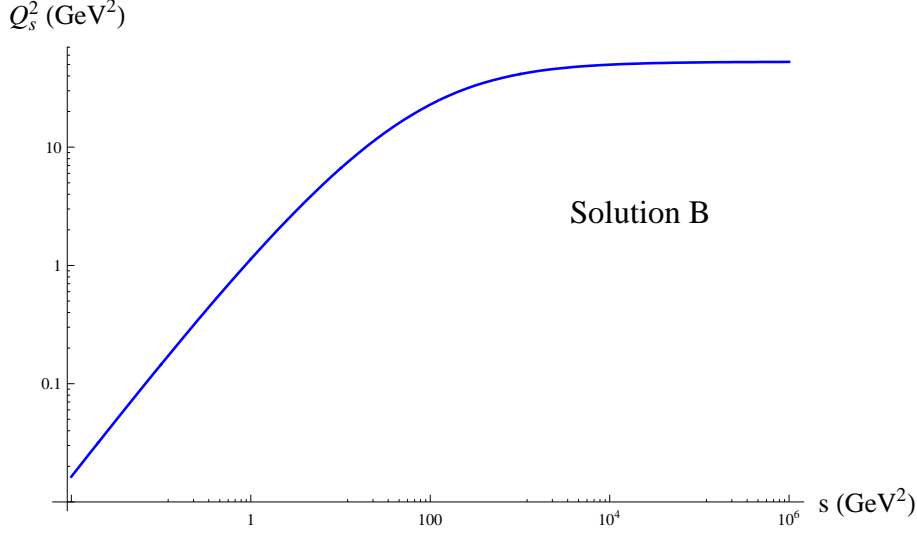


Figure 10: Saturation scale Q_s^2 as a function of the center-of-mass energy s for the amplitude plotted in Fig. 9 and corresponding to the same values of parameters as chosen for the solutions shown in Fig. 9. The saturation scale is obtained by imposing the condition $N(r = 1/Q_s, s) = 0.5$ on $N(r, s)$ in Eq. (4.30).

Let us study the low and high energy asymptotics of Eq. (4.30). $N(r, s)$ in Eq. (4.30) and in Fig. 9 becomes non-zero at $m = 4/27$ corresponding to

$$r = r^* \equiv \left(\frac{4}{27}\right)^{1/4} \frac{1}{c_0 \sqrt{s}}. \quad (4.32)$$

Expanding $N(r, s)$ from Eq. (4.30) for the $n = 0$ branch in $r - r^*$ yields

$$N(r, s) \Big|_{r-r^* \ll 1/\sqrt{s}, \quad r > r^*} \approx 1 - \exp \left\{ -\frac{\sqrt{\lambda} a 2^{1/4} s^{3/4}}{\pi c_0^{1/2} 3^{1/8}} \sqrt{r - r^*} \right\}. \quad (4.33)$$

(We have not expanded the exponent here and in previous expansions as a may be large.) As $r^* \sim 1/\sqrt{s}$, we obtain $Q_s^2 \sim 1/r^{*2} \sim s$, as observed in Eq. (4.31). The $Q_s^2 \sim s$ scaling is somewhat unusual, as in terms of x_{Bj} it implies the existence of saturation Bjorken- x , some x_{Bj}^{sat} , such that the saturation sets in for $x_{Bj} \leq x_{Bj}^{\text{sat}}$ independent of Q^2 . However, as the $Q_s^2 \sim s$ scaling is observed for large- x_{Bj} , we can not apply this conclusion for small- x_{Bj} physics, which we are studying using the Wilson loop.

One can easily check using Eqs. (4.6) and (4.30) that the $sr^2 \gg 1$ asymptotics of Eq. (4.30) is given by Eq. (4.27). Thus the high energy asymptotics of both possible solutions discussed here is the same. The saturation scale at large s is also the same for $n = 1$ branch and for the superposition of $n = 2$ and $n = 0$ branches. It is given by Eq. (4.28). Therefore, the main difference between the two possible solutions is at small r /low energy s .

Let us finally note that, in DIS, for the Wilson loop to span the whole shock wave in the longitudinal direction, the interaction of the $q\bar{q}$ pair should be coherent over the longitudinal length of the whole shock wave. In other words, in the rest frame of the nucleus, the longitudinal coherence length of the $q\bar{q}$ pair should be larger than the diameter of the nucleus. The standard condition for this to happen in DIS is (see [90] and references therein)

$$\frac{1}{2 m_N x_{Bj}} \gg 2 R \quad (4.34)$$

with m_N the nucleon mass. Omitting factors of 2, putting $m_N \sim \Lambda$ and using x_{Bj} from Eq. (4.20) yields

$$s r^2 \gg A^{1/3}. \quad (4.35)$$

Violation of this condition does not imply a breakdown of our approximation. It would only mean that the Wilson loop does not stretch across the whole shock wave in the longitudinal direction, but only over a part of it. This would imply that, when the condition (4.35) is violated, $A^{1/3}$ in our above expressions for $N(r, s)$ should be replaced by $s r^2$. While this prescription would modify some of our large- x_{Bj} conclusions above, such as Eq. (4.23) along with the shape of the rise of the saturation scale in Fig. 8, our main small- x_{Bj} conclusion of constant Q_s at high energy (4.28) would remain the same.

5. Conclusions

Let us restate our main results. We have studied DIS on a large nucleus in $\mathcal{N} = 4$ SYM using the AdS/CFT correspondence. We modeled the nucleus by an (infinitely) long shock wave. We argued that since for DIS in QCD the incoming virtual photon splits into a quark–anti-quark pair, which at high energies interacts with the nucleus eikonally (without recoil), the DIS cross section can be related to the expectation value of the Wilson loop, as shown in Eqs. (2.1), (2.2) and (2.3). We have calculated the expectation value of the Wilson loop by minimizing the area of the world-sheet for an open string connecting the quark and the anti-quark lines in the loop. We obtain two physically possible solutions resulting from different complex branches of string coordinates in the bulk. The two results for the forward scattering amplitude $N(r, s)$ are given in Eqs. (4.14) and (4.30), which are the main results of the paper. They are plotted in Figs. 7 and 9. The corresponding saturation scales are plotted as a function of energy in Figs. 8 and 10. In both cases the main feature is that the saturation scale becomes independent of energy/Bjorken- x at sufficiently high energies/small values of x_{Bj} .

We interpret this result as follows. At small gauge coupling, say in the BFKL evolution, each gluon emission is suppressed by a power of α_s , but is enhanced by a power of $\ln s$, which makes the resummations parameter $\alpha_s \ln s$ of the order of 1. High energy s is needed to generate

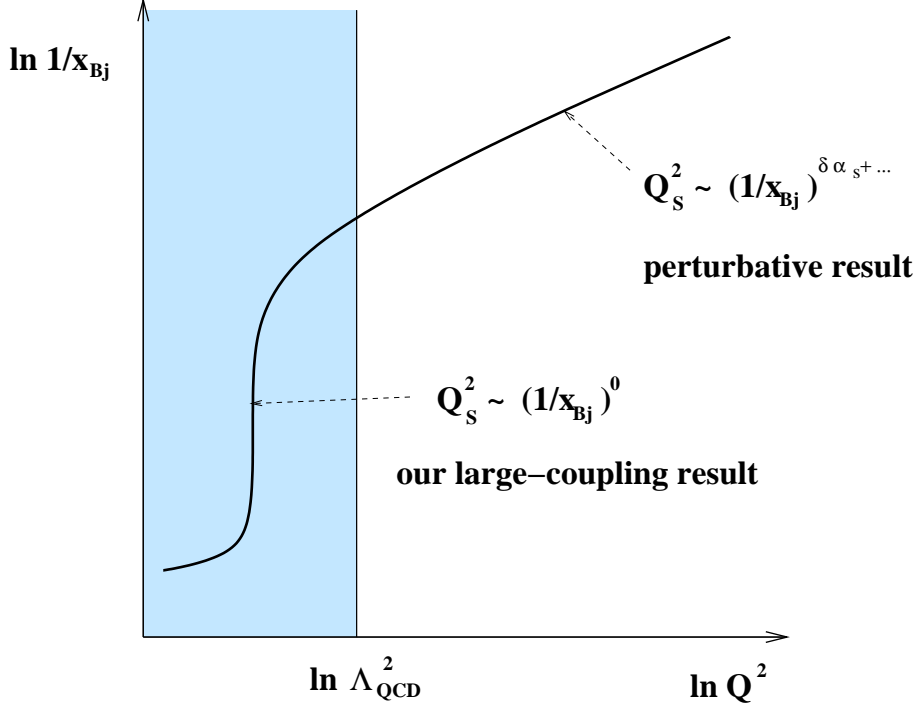


Figure 11: A sketch of the saturation line in the $(\ln Q^2, \ln 1/x_{Bj})$ plane. In the small coupling regime ($Q^2 \gg \Lambda_{\text{QCD}}^2$) the saturation scale grows according to CGC predictions. In the large coupling regime ($Q^2 \lesssim \Lambda_{\text{QCD}}^2$) the saturation scale is a constant function of x_{Bj} in accordance with our results in this work.

this enhancement. However, at large coupling the enhancement by logarithms (or by any other functions) of energy is not needed anymore, as $\lambda \gg 1$. Hence one might conjecture that at large λ partons fill up the whole phase space just due to sheer strength of the coupling. This way no energy enhancement is needed and increasing the energy should not change anything in this picture. This would lead to saturation scale being independent of energy.

As our calculation was done for $\mathcal{N} = 4$ SYM, it is important to understand its implications for QCD. In an effort to do so we have plotted the saturation line in the $(\ln Q^2, \ln 1/x_{Bj})$ plane in Fig. 11. The traditional physics of CGC happens in the small coupling regime of QCD for $Q^2 \gg \Lambda_{\text{QCD}}^2$, where Λ_{QCD} is the QCD confinement scale. The saturation scale there grows with $1/x_{Bj}$ as some power $Q_s^2 \sim (1/x_{Bj})^{\delta \alpha_s + \dots}$ in the LLA, with ellipsis denoting the higher order corrections. The strong coupling limit of QCD is $Q^2 \lesssim \Lambda_{\text{QCD}}^2$. If one assumes that the large-coupling analysis carried out in this paper is applicable to the non-perturbative large-coupling $Q^2 \lesssim \Lambda_{\text{QCD}}^2$ sector of QCD, then we can conclude that in this region $Q_s^2 \sim (1/x_{Bj})^0$. This is pictured in Fig. 11. In the non-perturbative region we have simply sketched the curve from Figs. 8 and 10: saturation scale starts out growing with decreasing x_{Bj} , but then levels off to a constant. As x_{Bj} decreases further, perturbative saturation mechanism would turn on and small transverse size partons would

be produced copiously due to $\ln 1/x_{Bj}$ enhancement, leading again to the saturation scale growing as a positive power of $1/x_{Bj}$. Indeed Fig. 11 is applicable only for a relatively small/dilute target, which would insure that there is a region of small x_{Bj} where Q_s^2 is still in the non-perturbative region. For a very large nucleus or at very high energies perturbative QCD effects would dominate making Q_s^2 perturbative. At the modern-day accelerators, such as HERA, Tevatron, RHIC, and LHC, one gets $Q_s \approx 1 \div 3$ GeV for protons and nuclei [36]. This scale may not be large enough to completely place us in the perturbative QCD region. Therefore it is likely that the physics at these machines lies in the transition region between the perturbative and non-perturbative regimes pictured in Fig. 11.

Addendum

After the paper was already in print, we realized that by modifying certain mathematical conventions one could obtain the dipole scattering amplitude $N(r)$ given in Fig. 9 from a *single branch* of the solution for z_{max} as opposed to the superposition of two branches described in Sect. 4.3. A more conventional definition of the Nambu-Goto action in Minkowski space is different by a minus sign from our Eq. (2.7). Using only the $n = 2$ root for z_{max} , denoted $z_{max}^{n=2}$, in such action along with Eq. (4.29) would lead to the dipole amplitude in Fig. 9. Alternatively, using the complex conjugate of the $n = 2$ root for z_{max} , denoted $z_{max}^{n=2*}$, in Eq. (4.30) would also give the dipole amplitude in Fig. 9 coming from a single branch of the solution. This observation does not modify any of the results in the paper (and in particular in Sect. 4.3).

Acknowledgments

We would like to thank Hong Liu, John McGreevy, Krishna Rajagopal, and Amit Sever for interesting discussions and for encouraging us to write this paper. We are also very grateful to Samir Mathur and Al Mueller for a number of very informative and supportive discussions. We thank Al Mueller for a careful reading of the manuscript.

This research is sponsored in part by the U.S. Department of Energy under Grant No. DE-FG02-05ER41377.

A. Monotonicity of $N(r, s)$ as a function of r

We wish to show that $N(r, s)$ appearing in Fig. 7 is a monotonic function of r for all s , and not just for the values of s used in the plot. In particular, we claim that $N(r, s)$ goes to zero when $r \rightarrow 0$ and $N(r, s)$ goes to 1 when $r \rightarrow \infty$ with a monotonic interpolation between the two extremes and without any local minima or maxima in-between. This would imply that $N(r, s)$ is not only monotonic, but in addition is restricted between zero and one, a necessary condition arising from unitarity.

The minimum requirement we need to prove is that the derivative of the expression in the square bracket in the exponential of (4.14) is positive for any (positive) values of r and s . We should have in mind that $\rho_{max} = \rho_{max}(r, s)$ [see Eqs. (4.12), (4.1-4.4)]. We denote by $E(r, s)$ the expression in the square brackets in the exponent of (4.14)

$$E(r, s) \equiv \frac{c_0^2 r^2}{\rho_{max}^3(r, s)} + \frac{2}{\rho_{max}(r, s)} - \frac{2}{z_h(s)}. \quad (\text{A1})$$

We proceed by evaluating its derivative with respect to r

$$\frac{\partial E}{\partial r} = - \left(\frac{3 c_0^2 r^2}{\rho_{max}^4} + \frac{2}{\rho_{max}^2} \right) \frac{\partial \rho_{max}}{\partial r} + \frac{2 c_0^2 r}{\rho_{max}^3} \quad (\text{A2})$$

At this point we recall that $z_{max} = i\rho_{max}$. Eq. (3.21) then gives

$$c_0^2 r^2 = s^2 \rho_{max}^6 - \rho_{max}^2. \quad (\text{A3})$$

Differentiating both sides of Eq. (A3) with respect to r we obtain

$$c_0^2 r = \rho_{max} (3 s^2 \rho_{max}^4 - 1) \frac{\partial \rho_{max}}{\partial r}. \quad (\text{A4})$$

Solving Eq. (A4) for $\frac{\partial \rho_{max}}{\partial r}$ and eliminating $\frac{\partial \rho_{max}}{\partial r}$ in Eq. (A2) yields

$$\frac{\rho_{max}^3}{c_0^2 r} \frac{\partial E}{\partial r} = - \frac{2 \rho_{max}^2 + 3 c_0^2 r^2}{3 s^2 \rho_{max}^6 - \rho_{max}^2} + 2. \quad (\text{A5})$$

We now eliminate ρ_{max}^6 in the denominator of Eq. (A5) using Eq. (A3). This yields

$$\frac{\rho_{max}^3}{c_0^2 r} \frac{\partial E}{\partial r} = - \frac{2 \rho_{max}^2 + 3 c_0^2 r^2}{3 (c_0^2 r^2 + \rho_{max}^2) - \rho_{max}^2} + 2 = 1 > 0. \quad (\text{A6})$$

This completes the proof of our statement. As can be easily shown (see also Fig. 5) $\rho_{max} > 0$. Therefore we conclude that

$$\frac{\partial E}{\partial r} > 0 \quad (\text{A7})$$

for all $r > 0$, which means that $N(r, s)$ in Eq. (4.14) is a monotonically increasing function of r .

References

- [1] L. V. Gribov, E. M. Levin, and M. G. Ryskin, *Semihard Processes in QCD*, *Phys. Rept.* **100** (1983) 1–150.
- [2] A. H. Mueller and J.-w. Qiu, *Gluon recombination and shadowing at small values of x* , *Nucl. Phys.* **B268** (1986) 427.

- [3] L. D. McLerran and R. Venugopalan, *Green's functions in the color field of a large nucleus*, *Phys. Rev.* **D50** (1994) 2225–2233, [[hep-ph/9402335](#)].
- [4] L. D. McLerran and R. Venugopalan, *Gluon distribution functions for very large nuclei at small transverse momentum*, *Phys. Rev.* **D49** (1994) 3352–3355, [[hep-ph/9311205](#)].
- [5] L. D. McLerran and R. Venugopalan, *Computing quark and gluon distribution functions for very large nuclei*, *Phys. Rev.* **D49** (1994) 2233–2241, [[hep-ph/9309289](#)].
- [6] Y. V. Kovchegov, *Non-abelian Weizsaecker-Williams field and a two- dimensional effective color charge density for a very large nucleus*, *Phys. Rev.* **D54** (1996) 5463–5469, [[hep-ph/9605446](#)].
- [7] Y. V. Kovchegov, *Quantum structure of the non-abelian Weizsaecker-Williams field for a very large nucleus*, *Phys. Rev.* **D55** (1997) 5445–5455, [[hep-ph/9701229](#)].
- [8] J. Jalilian-Marian, A. Kovner, L. D. McLerran, and H. Weigert, *The intrinsic glue distribution at very small x* , *Phys. Rev.* **D55** (1997) 5414–5428, [[hep-ph/9606337](#)].
- [9] J. Jalilian-Marian, A. Kovner, A. Leonidov, and H. Weigert, *The BFKL equation from the Wilson renormalization group*, *Nucl. Phys.* **B504** (1997) 415–431, [[hep-ph/9701284](#)].
- [10] J. Jalilian-Marian, A. Kovner, A. Leonidov, and H. Weigert, *The Wilson renormalization group for low x physics: Towards the high density regime*, *Phys. Rev.* **D59** (1998) 014014, [[hep-ph/9706377](#)].
- [11] J. Jalilian-Marian, A. Kovner, and H. Weigert, *The Wilson renormalization group for low x physics: Gluon evolution at finite parton density*, *Phys. Rev.* **D59** (1998) 014015, [[hep-ph/9709432](#)].
- [12] J. Jalilian-Marian, A. Kovner, A. Leonidov, and H. Weigert, *Unitarization of gluon distribution in the doubly logarithmic regime at high density*, *Phys. Rev.* **D59** (1999) 034007, [[hep-ph/9807462](#)].
- [13] A. Kovner, J. G. Milhano, and H. Weigert, *Relating different approaches to nonlinear QCD evolution at finite gluon density*, *Phys. Rev.* **D62** (2000) 114005, [[hep-ph/0004014](#)].
- [14] H. Weigert, *Unitarity at small Bjorken x* , *Nucl. Phys.* **A703** (2002) 823–860, [[hep-ph/0004044](#)].
- [15] E. Iancu, A. Leonidov, and L. D. McLerran, *Nonlinear gluon evolution in the color glass condensate. I*, *Nucl. Phys.* **A692** (2001) 583–645, [[hep-ph/0011241](#)].
- [16] E. Ferreiro, E. Iancu, A. Leonidov, and L. McLerran, *Nonlinear gluon evolution in the color glass condensate. II*, *Nucl. Phys.* **A703** (2002) 489–538, [[hep-ph/0109115](#)].
- [17] Y. V. Kovchegov, *Small- x F_2 structure function of a nucleus including multiple pomeron exchanges*, *Phys. Rev.* **D60** (1999) 034008, [[hep-ph/9901281](#)].
- [18] Y. V. Kovchegov, *Unitarization of the BFKL pomeron on a nucleus*, *Phys. Rev.* **D61** (2000) 074018, [[hep-ph/9905214](#)].

- [19] I. Balitsky, *Operator expansion for high-energy scattering*, *Nucl. Phys.* **B463** (1996) 99–160, [hep-ph/9509348].
- [20] I. Balitsky, *Operator expansion for diffractive high-energy scattering*, hep-ph/9706411.
- [21] I. Balitsky, *Factorization and high-energy effective action*, *Phys. Rev.* **D60** (1999) 014020, [hep-ph/9812311].
- [22] E. Iancu and R. Venugopalan, *The color glass condensate and high energy scattering in QCD*, hep-ph/0303204.
- [23] H. Weigert, *Evolution at small x_{bj} : The Color Glass Condensate*, *Prog. Part. Nucl. Phys.* **55** (2005) 461–565, [hep-ph/0501087].
- [24] J. Jalilian-Marian and Y. V. Kovchegov, *Saturation physics and deuteron gold collisions at RHIC*, *Prog. Part. Nucl. Phys.* **56** (2006) 104–231, [hep-ph/0505052].
- [25] A. H. Mueller, *Small x Behavior and Parton Saturation: A QCD Model*, *Nucl. Phys.* **B335** (1990) 115.
- [26] E. A. Kuraev, L. N. Lipatov, and V. S. Fadin, *The Pomernanchuk singularity in non-Abelian gauge theories*, *Sov. Phys. JETP* **45** (1977) 199–204.
- [27] Y. Y. Balitsky and L. N. Lipatov *Sov. J. Nucl. Phys.* **28** (1978) 822.
- [28] E. Iancu, K. Itakura, and L. McLerran, *Geometric scaling above the saturation scale*, *Nucl. Phys.* **A708** (2002) 327–352, [hep-ph/0203137].
- [29] J. L. Albacete, N. Armesto, J. G. Milhano, C. A. Salgado, and U. A. Wiedemann, *Numerical analysis of the Balitsky-Kovchegov equation with running coupling: Dependence of the saturation scale on nuclear size and rapidity*, *Phys. Rev.* **D71** (2005) 014003, [hep-ph/0408216].
- [30] D. Kharzeev and M. Nardi, *Hadron production in nuclear collisions at RHIC and high density QCD*, *Phys. Lett.* **B507** (2001) 121–128, [nucl-th/0012025].
- [31] D. Kharzeev, E. Levin, and M. Nardi, *The onset of classical QCD dynamics in relativistic heavy ion collisions*, *Phys. Rev.* **C71** (2005) 054903, [hep-ph/0111315].
- [32] D. Kharzeev, E. Levin, and L. McLerran, *Parton saturation and $N(\text{part})$ scaling of semi-hard processes in QCD*, *Phys. Lett.* **B561** (2003) 93–101, [hep-ph/0210332].
- [33] J. L. Albacete, N. Armesto, A. Kovner, C. A. Salgado, and U. A. Wiedemann, *Energy dependence of the Cronin effect from non-linear QCD evolution*, *Phys. Rev. Lett.* **92** (2004) 082001, [hep-ph/0307179].
- [34] D. Kharzeev, Y. V. Kovchegov, and K. Tuchin, *Cronin effect and high- $p(t)$ suppression in p a collisions*, *Phys. Rev.* **D68** (2003) 094013, [hep-ph/0307037].

- [35] D. Kharzeev, Y. V. Kovchegov, and K. Tuchin, *Nuclear modification factor in $d + Au$ collisions: Onset of suppression in the color glass condensate*, *Phys. Lett.* **B599** (2004) 23–31, [[hep-ph/0405045](#)].
- [36] J. L. Albacete, *Particle multiplicities in Lead-Lead collisions at the LHC from non-linear evolution with running coupling*, *Phys. Rev. Lett.* **99** (2007) 262301, [[arXiv:0707.2545](#)].
- [37] V. S. Fadin and L. N. Lipatov, *BFKL pomeron in the next-to-leading approximation*, *Phys. Lett.* **B429** (1998) 127–134, [[hep-ph/9802290](#)].
- [38] M. Ciafaloni and G. Camici, *Energy scale(s) and next-to-leading BFKL equation*, *Phys. Lett.* **B430** (1998) 349–354, [[hep-ph/9803389](#)].
- [39] I. Balitsky and G. A. Chirilli, *Next-to-leading order evolution of color dipoles*, *Phys. Rev.* **D77** (2008) 014019, [[arXiv:0710.4330](#)].
- [40] D. A. Ross, *The effect of higher order corrections to the bfkL equation on the perturbative pomeron*, *Phys. Lett.* **B431** (1998) 161–165, [[hep-ph/9804332](#)].
- [41] Y. V. Kovchegov and A. H. Mueller, *Running coupling effects in BFKL evolution*, *Phys. Lett.* **B439** (1998) 428–436, [[hep-ph/9805208](#)].
- [42] M. Ciafaloni, D. Colferai, and G. P. Salam, *Renormalization group improved small- x equation*, *Phys. Rev.* **D60** (1999) 114036, [[hep-ph/9905566](#)].
- [43] I. I. Balitsky, *Quark Contribution to the Small- x Evolution of Color Dipole*, *Phys. Rev. D* **75** (2007) 014001, [[hep-ph/0609105](#)].
- [44] Y. Kovchegov and H. Weigert, *Triumvirate of Running Couplings in Small- x Evolution*, *Nucl. Phys.* **A 784** (2007) 188–226, [[hep-ph/0609090](#)].
- [45] E. Gardi, J. Kuokkanen, K. Rummukainen, and H. Weigert, *Running coupling and power corrections in nonlinear evolution at the high-energy limit*, *Nucl. Phys.* **A784** (2007) 282–340, [[hep-ph/0609087](#)].
- [46] Y. V. Kovchegov and H. Weigert, *Quark loop contribution to BFKL evolution: Running coupling and leading- $N(f)$ NLO intercept, accepted for publication at Nucl. Phys. A* (2006) [[hep-ph/0612071](#)].
- [47] J. L. Albacete and Y. V. Kovchegov, *Solving high energy evolution equation including running coupling corrections*, *Phys. Rev.* **D75** (2007) 125021, [[0704.0612](#)].
- [48] J. M. Maldacena, *The large n limit of superconformal field theories and supergravity*, *Adv. Theor. Math. Phys.* **2** (1998) 231–252, [[hep-th/9711200](#)].
- [49] S. S. Gubser, I. R. Klebanov, and A. M. Polyakov, *Gauge theory correlators from non-critical string theory*, *Phys. Lett.* **B428** (1998) 105–114, [[hep-th/9802109](#)].
- [50] E. Witten, *Anti-de sitter space and holography*, *Adv. Theor. Math. Phys.* **2** (1998) 253–291, [[hep-th/9802150](#)].

- [51] O. Aharony, S. S. Gubser, J. M. Maldacena, H. Ooguri, and Y. Oz, *Large n field theories, string theory and gravity*, *Phys. Rept.* **323** (2000) 183–386, [[hep-th/9905111](#)].
- [52] R. A. Janik and R. B. Peschanski, *High energy scattering and the AdS/CFT correspondence*, *Nucl. Phys.* **B565** (2000) 193–209, [[hep-th/9907177](#)].
- [53] J. Polchinski and M. J. Strassler, *The string dual of a confining four-dimensional gauge theory*, [hep-th/0003136](#).
- [54] J. Polchinski and M. J. Strassler, *Deep inelastic scattering and gauge/string duality*, *JHEP* **05** (2003) 012, [[hep-th/0209211](#)].
- [55] C. A. Ballon Bayona, H. Boschi-Filho, and N. R. F. Braga, *Deep inelastic scattering from gauge string duality in the soft wall model*, *JHEP* **03** (2008) 064, [[arXiv:0711.0221](#)].
- [56] C. A. Ballon Bayona, H. Boschi-Filho, and N. R. F. Braga, *Deep inelastic structure functions from supergravity at small x* , [arXiv:0712.3530](#).
- [57] R. C. Brower, J. Polchinski, M. J. Strassler, and C.-I. Tan, *The Pomeron and Gauge/String Duality*, *JHEP* **12** (2007) 005, [[hep-th/0603115](#)].
- [58] A. M. Stasto, *The BFKL Pomeron in the weak and strong coupling limits and kinematical constraints*, *Phys. Rev.* **D75** (2007) 054023, [[hep-ph/0702195](#)].
- [59] A. Donnachie and P. V. Landshoff, *Small x : Two pomerons!*, *Phys. Lett.* **B437** (1998) 408–416, [[hep-ph/9806344](#)].
- [60] Y. Hatta, E. Iancu, and A. H. Mueller, *Deep inelastic scattering at strong coupling from gauge/string duality : the saturation line*, *JHEP* **01** (2008) 026, [[arXiv:0710.2148](#)].
- [61] Y. Hatta, E. Iancu, and A. H. Mueller, *Deep inelastic scattering off a $N=4$ SYM plasma at strong coupling*, *JHEP* **01** (2008) 063, [[arXiv:0710.5297](#)].
- [62] J. M. Maldacena, *Wilson loops in large N field theories*, *Phys. Rev. Lett.* **80** (1998) 4859–4862, [[hep-th/9803002](#)].
- [63] S.-J. Rey, S. Theisen, and J.-T. Yee, *Wilson-Polyakov loop at finite temperature in large N gauge theory and anti-de Sitter supergravity*, *Nucl. Phys.* **B527** (1998) 171–186, [[hep-th/9803135](#)].
- [64] S.-J. Rey and J.-T. Yee, *Macroscopic strings as heavy quarks in large N gauge theory and anti-de Sitter supergravity*, *Eur. Phys. J.* **C22** (2001) 379–394, [[hep-th/9803001](#)].
- [65] J. Sonnenschein, *What does the string / gauge correspondence teach us about Wilson loops?*, [hep-th/0003032](#).
- [66] H. Liu, K. Rajagopal, and U. A. Wiedemann, *Calculating the jet quenching parameter from AdS/CFT*, *Phys. Rev. Lett.* **97** (2006) 182301, [[hep-ph/0605178](#)].

- [67] H. Liu, K. Rajagopal, and U. A. Wiedemann, *An AdS/CFT calculation of screening in a hot wind*, *Phys. Rev. Lett.* **98** (2007) 182301, [[hep-ph/0607062](#)].
- [68] H. Liu, K. Rajagopal, and U. A. Wiedemann, *Wilson loops in heavy ion collisions and their calculation in AdS/CFT*, *JHEP* **03** (2007) 066, [[hep-ph/0612168](#)].
- [69] P. C. Argyres, M. Edalati, and J. F. Vazquez-Poritz, *Lightlike Wilson loops from AdS/CFT*, *JHEP* **03** (2008) 071, [[arXiv:0801.4594](#)].
- [70] P. C. Argyres, M. Edalati, and J. F. Vazquez-Poritz, *No-drag string configurations for steadily moving quark- antiquark pairs in a thermal bath*, *JHEP* **01** (2007) 105, [[hep-th/0608118](#)].
- [71] P. C. Argyres, M. Edalati, and J. F. Vazquez-Poritz, *Spacelike strings and jet quenching from a Wilson loop*, *JHEP* **04** (2007) 049, [[hep-th/0612157](#)].
- [72] S. S. Gubser, S. S. Pufu, and A. Yarom, *Shock waves from heavy-quark mesons in AdS/CFT*, [arXiv:0711.1415](#).
- [73] R. Ishizeki, M. Kruczenski, and A. Tirziu, *New open string solutions in AdS5*, [arXiv:0804.3438](#).
- [74] M. Chernicoff, J. A. Garcia, and A. Guijosa, *The energy of a moving quark-antiquark pair in an $N = 4$ SYM plasma*, *JHEP* **09** (2006) 068, [[hep-th/0607089](#)].
- [75] M. Chernicoff and A. Guijosa, *Acceleration, Energy Loss and Screening in Strongly- Coupled Gauge Theories*, *JHEP* **06** (2008) 005, [[arXiv:0803.3070](#)].
- [76] L. D. Landau and E. M. Lifshitz, *Quantum mechanics, non-relativistic theory*, . vol. 3, Amsterdam ; Boston : Butterworth-Heinemann, (2003).
- [77] L. Fidkowski, V. Hubeny, M. Kleban, and S. Shenker, *The black hole singularity in AdS/CFT*, *JHEP* **02** (2004) 014, [[hep-th/0306170](#)].
- [78] D. Kharzeev, E. Levin, and M. Nardi, *Hadron multiplicities at the LHC*, [arXiv:0707.0811](#).
- [79] N. N. Nikolaev and B. G. Zakharov, *Colour transparency and scaling properties of nuclear shadowing in deep inelastic scattering*, *Z. Phys.* **C49** (1991) 607–618.
- [80] B. Z. Kopeliovich, J. Nemchick, N. N. Nikolaev, and B. G. Zakharov, *Novel color transparency effect: Scanning the wave function of vector mesons*, *Phys. Lett.* **B309** (1993) 179–186, [[hep-ph/9305225](#)].
- [81] G. P. Lepage and S. J. Brodsky, *Exclusive processes in perturbative quantum chromodynamics*, *Phys. Rev.* **D22** (1980) 2157.
- [82] S. J. Brodsky, H.-C. Pauli, and S. S. Pinsky, *Quantum chromodynamics and other field theories on the light cone*, *Phys. Rept.* **301** (1998) 299–486, [[hep-ph/9705477](#)].
- [83] Y. V. Kovchegov and L. D. McLerran, *Diffraction structure function in a quasi-classical approximation*, *Phys. Rev.* **D60** (1999) 054025, [[hep-ph/9903246](#)].

- [84] V. S. Fadin and A. D. Martin, *Infrared safety of impact factors for colorless particle interactions*, *Phys. Rev.* **D60** (1999) 114008, [[hep-ph/9904505](#)].
- [85] R. A. Janik and R. Peschanski, *Asymptotic perfect fluid dynamics as a consequence of AdS/CFT*, *Phys. Rev.* **D73** (2006) 045013, [[hep-th/0512162](#)].
- [86] S. de Haro, S. N. Solodukhin, and K. Skenderis, *Holographic reconstruction of spacetime and renormalization in the AdS/CFT correspondence*, *Commun. Math. Phys.* **217** (2001) 595–622, [[hep-th/0002230](#)].
- [87] D. Z. Fefferman and C. R. Graham, *Conformal invariants, Elie Cartan et les Mathématiques d’aujourd’hui* (Astérisque, 1985) 95.
- [88] J. L. Albacete, Y. V. Kovchegov, and A. Taliotis, *Modeling Heavy Ion Collisions in AdS/CFT*, [arXiv:0805.2927](#).
- [89] F. Dominguez, C. Marquet, A. H. Mueller, B. Wu, and B.-W. Xiao, *Comparing energy loss and p_{\perp} -broadening in perturbative QCD with strong coupling $\mathcal{N} = 4$ SYM theory*, [arXiv:0803.3234](#).
- [90] Y. V. Kovchegov and M. Strikman, *Ioffe time in double logarithmic approximation*, *Phys. Lett.* **B516** (2001) 314–320, [[hep-ph/0107015](#)].